https://doi.org/10.5194/egusphere-2026-2776
Preprint. Discussion started: 15 June 2026

Sensitivity of dynamic aging on the climate effects of black carbon aerosols over East Asia in summer

Peng Gao[1], Bingliang Zhuang[1,*], Yaxin Hu[1], Yinan Zhou[1], Runqi Zhao[1], Qianqian Wang[1], Shu Li[1], Tijian Wang[1], Mengmeng Li[1], Min Xie[2]

[1]School of Atmospheric Sciences, CMA-NJU Joint Laboratory for Climate Prediction Studies, Jiangsu Collaborative Innovation Center for Climate Change, Nanjing University, Nanjing 210023, Jiangsu, China
[2]School of Environment, Nanjing Normal University, Nanjing 210023, Jiangsu, China
*Corresponding author: Bingliang Zhuang (blzhuang@nju.edu.cn)

Abstract

The climate effects of black carbon (BC) remain highly uncertain, and one critical process that requires accurate representation in climate models is BC aging. This study implements a dynamic aging scheme, which accounts for both condensation and coagulation processes, into the regional climate and chemistry coupled model RegCM-Chem to evaluate the BC climate effects over East Asia in summer. Results indicate that in heavily polluted regions such as the North China Plain and the Sichuan Basin, the BC aging timescale is shorter than 10 hours, promoting the formation and wet deposition of hydrophilic BC, which reduces the BC column burden over East Asia by an average of 0.12 mg m^{-2}. Conversely, BC surface concentrations and optical depth exhibit an increase over eastern China due to the compensation of reduced dry deposition. The strengthened BC direct effects favor the development of the East Asian summer monsoon and enhance moisture convergence and cloud fraction in southern China. Additionally, accelerated aging also promotes increases in cloud droplet number concentrations and cloud optical depth. Under the dynamic aging scheme, the effective radiative forcing at the top of the atmosphere over East Asia due to BC–radiation interactions, BC–cloud interactions and BC–radiation–cloud interactions are +3.60, −0.58 and +0.90 W m^{-2}, respectively. The climate effects of BC exhibit pronounced nonlinearity driven by adjustments in circulation and cloud. Overall, BC induces a much drier and warmer surface in northern China, whereas southern China experiences the opposite effect.

https://doi.org/10.5194/egusphere-2026-2776
Preprint. Discussion started: 15 June 2026

1. Introduction

Black carbon aerosols (BC), mainly generated from the incomplete combustion processes such as fossil fuel and biomass burning (Bond et al., 2013), can exert unique and crucial influences on global and regional climate through direct (Ramanathan and Carmichael, 2008), semi-direct (Koch and Del Genio, 2010) and indirect effects (Zhuang et al., 2013). As a short-lived climate pollutant, BC is widely recognized as the second most important contributor to global warming after carbon dioxide (Jacobson, 2002). Moreover, BC-induced heating can alter atmospheric stability and thereby exacerbate air pollution levels (Randles and Ramaswamy, 2008; Ding et al., 2016).

Due to its high climate sensitivity and severe air pollution, East Asia is a region where aerosols have been firmly established as one of the primary anthropogenic factors of local climate change (Watson-Parris and Smith, 2022; Li et al., 2022; Zhuang et al., 2023). The Intergovernmental Panel on Climate Change Sixth Assessment Report evaluated the global effective radiative forcing of BC to range from −0.28 to +0.41 W m^{-2} (IPCC, 2021). At the regional scale, the mean direct radiative forcing due to BC was estimated at +0.84 W m^{-2} over East Asia (Gao et al., 2024) and +1.22 W m^{-2} over China (Li et al., 2016). This positive radiative forcing can substantially offset the cooling effect of scattering aerosols, thereby contributing to regional warming (Shindell and Faluvegi, 2009; Zhuang et al., 2019). Given that East Asia is dominated by an active summer monsoon system, the radiative perturbations exerted by BC further significantly modulate the atmospheric thermodynamic field and hydrological cycle (Zhang et al., 2009; Chen et al., 2024; Zhuang et al., 2025). For example, BC emissions from China may favor the circulation development of the East Asian summer monsoon (Wang et al., 2015; Zhuang et al., 2018a), consequently triggering regional droughts and floods over East Asia (Menon et al., 2002; Chen et al., 2020; Fang et al., 2025). All these studies have demonstrated the importance of BC to the energy balance of the Earth–atmosphere system and climate change, particularly in highly polluted and climate-sensitive areas.

Significant uncertainties persist in the assessment of the BC climate effects within current climate models, and precise quantification relies heavily on the representation of BC loadings, optical properties and hygroscopicity (Myhre et al., 2013; Fierce et al., 2017; Sand et al., 2021;Guan et al., 2026). A review by Bond et al. (2013) indicated that across 18 global climate models, the global BC column burden ranged from 0.11 to 0.53 mg m^{-2}, with corresponding BC absorption aerosol optical depth (AAOD) at 500 nm varying between 0.0006 and 0.0035. Furthermore, the indirect radiative forcing induced by BC in liquid clouds is estimated to range from −0.64 to +0.23 W m^{-2} (Koch et al., 2011; Storelvmo, 2012; Zhang et al., 2025). Such discrepancies in simulations principally arise from the different treatments of aerosol processes, among which the BC aging is a key process that requires faithful representations (Lund et al., 2017; Shen et al., 2024). Freshly emitted BC particles typically exhibit hydrophobic characteristics (Weingartner et al., 1997). Through a series of complex atmospheric processes, such as condensation and coagulation, they evolve into aged, hydrophilic and internally mixed ones. This transformation, known as the “aging process”, leads to changes in the BC physical and optical properties (Johnson et al., 2005; Kanakidou et al., 2005; Dusek et al., 2006). The increased BC hygroscopicity due to the aging process promotes their activation efficiency as cloud condensation nuclei (CCN) and subsequent wet removal of BC particles (Zuberi et al., 2005; Furutani et al., 2008; Lund et al., 2018). For instance, a relatively thin soluble coating as thin as 2 nm is enough to trigger hydrophobic BC particles CCN-active under typical atmospheric

https://doi.org/10.5194/egusphere-2026-2776
Preprint. Discussion started: 15 June 2026

supersaturation conditions (Dalirian et al., 2018). Additionally, when internally mixed with other coating materials, the light absorption capacity of BC can be enhanced by a factor of 1–3 due to the "lensing effect", which is critical for accurately assessing the BC optical properties and direct radiative forcing (Lack et al., 2012; Cappa et al., 2012; Chakrabarty and Heinson, 2018; Wang et al., 2023). These findings highlight that both the direct and indirect climate effects of BC are highly sensitive to the aging process in climate models.

Simulating the evolution of complex particle populations over time remains a significant challenge in Earth system models (Bauer et al., 2008). Currently, the most accurate simulations of BC aging and mixing state are achieved using particle-resolved models that track the size and chemical composition of individual particles. A prominent example is PartMC-MOSAIC, developed by Riemer et al. (2009) and Riemer et al. (2019), which explicitly resolves the aerosol mixing state. However, its application in large-scale simulations is still constrained by prohibitive computational costs and storage requirements. Consequently, most climate models represent BC aging via highly parameterized methods within simplified aerosol modules (Fierce et al., 2017). Many models employ two tracers for BC, corresponding to fresh and aged BC (hydrophobic and hydrophilic BC), and assume that fresh BC is converted to aged BC using a characteristic *e*-folding aging timescale (Cooke et al., 1999; Chung and Seinfeld, 2002). In the simplest treatment, this aging timescale is often set to a fixed value of approximately one day (Solmon et al., 2006; Koch et al., 2009; Lee et al., 2013). Such an assumption, however, neglects the fact that BC aging rates vary substantially across regions under different atmospheric conditions. Peng et al. (2016) measured the BC aging timescale of 4.6 hours in Beijing and 18 hours in Houston, respectively, by the QUALITY chamber. Similarly, in highly urbanized environments like Los Angeles (Krasowsky et al., 2016) and Mexico City (Moffet and Prather, 2009), BC particles could become largely aged within about three hours. Numerical simulations by Ghosh et al. (2021) and Shen et al. (2023) both showed that the BC aging timescale typically spanned only a few hours across the highly polluted regions of eastern China, whereas it was significantly protracted in the Qinghai–Tibet Plateau, often exceeding 24 hours. Recently, Fierce et al. (2025) quantified the average timescale for internal mixing as approximately 3 hours in a global aerosol model, which is much shorter than the default setting traditionally applied in bulk aerosol models.

To address these issues, this study incorporates a dynamic BC aging parameterization that explicitly accounts for condensation and coagulation processes into the regional climate and chemistry coupled model RegCM-Chem. A series of numerical experiments are conducted to systematically investigate the impacts of dynamic aging representation on the direct, indirect and total climate effects of BC over East Asia during summer. Particular attention is given to the responses of BC loading, radiative forcing and regional climate to dynamic aging. This study aims to provide a more realistic assessment of BC climate effects in highly polluted and monsoon-dominated East Asia and to improve the understanding of uncertainties associated with BC aging processes in regional climate simulations. In the following, section 2 describes the dynamic aging scheme and the experimental design, section 3 presents the key findings and section 4 is the conclusion.

2. Method

2.1 Model description

https://doi.org/10.5194/egusphere-2026-2776
Preprint. Discussion started: 15 June 2026

Compared with global models, regional climate models offer higher spatial resolution and a greater capability to capture small-scale climatic features (Denis et al., 2002). Here, we employ the regional climate and chemistry coupled model (RegCM-Chem), developed by the Abdus Salam International Centre for Theoretical Physics (ICTP), to assess the climate effects of BC over East Asia. In recent years, RegCM-Chem has been widely applied in studies of the regional aerosol–climate interactions (Ghosh et al., 2023; Ma et al., 2023; Hu et al., 2024; Cao et al., 2026). To better address trace gases, inorganic and secondary organic aerosols, a gas phase chemistry module with a Carbon-Bond Mechanism version Z (Shalaby et al., 2012), a thermodynamic equilibrium model ISORROPIA (Fountoukis and Nenes, 2007) and a volatility basis set model (Yin et al., 2015) have been coupled into the model. Additionally, the current version of RegCM-Chem also involves new physical parameterization schemes, such as those for land surface, planetary boundary layer and air–sea flux (Giorgi et al., 2012). The radiation transfer package from the National Center for Atmospheric Research Community Climate Model, version 3 is adopted to investigate the direct radiative forcing of aerosols (Kiehl et al., 1996).

The aerosol module in RegCM-Chem incorporates hydrophobic and hydrophilic BC and organic carbon (OC), as well as a sulfate aerosol scheme described in Qian et al. (2001). The mass concentrations of these species are tracked independently, and they are assumed to be externally mixed. For a given tracer *i*, the rate of change in its mass mixing ratio is governed by the following tracer transport equation (Solmon et al., 2006):

$$\frac{\partial m^i}{\partial t} = -\bar{V}\cdot\nabla m^i + F_H^i + F_V^i + T_C^i + E^i - R_{Wls}^i - R_{Wc}^i - D_d^i + \sum\left(Q_p^i - Q_l^i\right), \quad (1)$$

where the first four terms represent advection, horizontal and vertical turbulent diffusion, and convective transport, respectively. The surface emission term E^i will be detailed in the subsequent section. R_{Wls}^i and R_{Wc}^i are the wet removal rates associated with large-scale and convective rain, respectively, and D_d^i denotes the dry deposition. The final term $\sum\left(Q_p^i - Q_l^i\right)$ for BC represents production and loss due to the aging process, which is simplified in the current scheme as a transformation from a hydrophobic to a hydrophilic state with a fixed e-folding timescale of τ_0=1.15 days (27.6 hours) (Cooke et al., 1999). The atmospheric lifetime of aerosols is primarily determined by dry and wet deposition processes. In RegCM-Chem, the dry deposition flux is computed from the tracer concentration in the model's lowest layer and the dry deposition velocity depending on particle physical properties and aerodynamic transport mechanisms (Giorgi, 1986; Zakey et al., 2008). Wet deposition in the model is divided into in-cloud and below-cloud scavenging. The in-cloud scavenging process occurs in large-scale clouds when the liquid water in the model layers with a nonzero cloud fraction exceeds a prescribed threshold, and it is parameterized as a function of the fractional removal rate of the liquid water and aerosol solubility (Ghosh et al., 2023). Different aerosol solubilities are assigned to hydrophobic and hydrophilic particles, thereby distinguishing their in-cloud scavenging rates. The below-cloud scavenging is determined by the precipitation rate and particle collection efficiency, the latter of which is calculated from the aerosol effective diameter and density (Giorgi, 1989; Nair et al., 2012).

2.2 Dynamic aging scheme

Based on the work of Fierce et al. (2017) and Ghosh et al. (2021), we replace the currently adopted 1.15-day fixed aging timescale in RegCM-Chem with a dynamic BC aging parameterization. Fierce

https://doi.org/10.5194/egusphere-2026-2776
Preprint. Discussion started: 15 June 2026

et al. (2017) used a high-detail particle-resolved model to simulate the aging evolution of aerosols through condensation and coagulation processes. Through parameter regression, the required timescale for the transition to achieve internal mixing is expressed as a function of the condensation rate I_{cond} and the overall aerosol number concentration N:

$$\tau_{mix} = \frac{1}{I_{cond} \cdot k_{cond} + N \cdot k_{coag}}, \quad (2)$$

where the parameters k_{cond} = 0.1 nm^{-1} and k_{coag} = 6 × 10^{-6} cm^3 h^{-1} were obtained by least-squares regression using the outputs from hundreds of particle-resolved simulations covering a wide range of aging conditions, considering the effect of condensation and coagulation individually. Simulations involving the combined processes are used to validate the parameterization, as described in detail by Fierce et al. (2017). Following Ghosh et al. (2021), the total aerosol number concentration N is calculated using the following equation:

$$N = \Sigma \frac{M}{D^3 \cdot \rho \cdot \frac{\pi}{6}}, \quad (3)$$

where M, D and ρ represent the mass concentration, characteristic effective diameter, and density of a specific tracer, respectively. The condensation growth term I_{cond} in Eq. (1) is determined as follows:

$$I_{cond} = \frac{\left.\frac{\partial m_{SO_4}}{\partial t}\right|_{cond}}{\rho_{SO_4} \cdot S_{aer}}, \quad (4)$$

where $\left.\frac{\partial m_{SO_4}}{\partial t}\right|_{cond}$ and S_{aer} are the condensation mass flux of sulfate and the surface area concentration of aerosols, respectively. Detailed information of the aging scheme can be found in Fierce et al. (2017) and Ghosh et al. (2021).

2.3 BC direct and indirect effects

The direct radiative effect of aerosols is highly dependent on aerosol optical depth (AOD). The BC AOD $\alpha_i(\lambda)$ at different wavelengths λ in RegCM-Chem is calculated according to the following formula (Kasten, 1969; Kiehl and Briegleb, 1993; Kiehl et al., 2000):

$$\alpha_i(\lambda) = M_i \sigma_{\lambda i} f(RH), \quad (5)$$

where M_i is the mass concentration of a specific tracer i (including hydrophobic/fresh and hydrophilic/aged BC). $\sigma_{\lambda i}$ denotes the wavelength-dependent mass extinction coefficient, which is derived from the refractive index and lognormal size distribution based on a Mie code (Matzler, 2002). $f(RH)$ represents the hygroscopic growth factor and differs among aerosol species. Further descriptions are provided in Solmon et al. (2006) and Huang et al. (2007).

To address the aerosol first indirect effect, the cloud droplet activation parameterization of Abdul-Razzak and Ghan (2000, 2002) is further developed, in which the cloud droplet number concentration N_d is expressed as follows:

$$N_d = \sum_i N_i \times \frac{1}{2}[1 - erf(u_i)], \quad (6)$$

$$u_i = \frac{2 \times \ln\left(\frac{S_{mi}}{S_{max}}\right)}{3\sqrt{2} \times ln\sigma_i}, \quad (7)$$

https://doi.org/10.5194/egusphere-2026-2776
Preprint. Discussion started: 15 June 2026

where N_i, S_{mi} and σ_i denote the number concentration, critical supersaturation and geometric standard deviation of tracer *i*, respectively. S_{mi} is determined by the coefficient of the curvature effect and hygroscopicity. Previous studies generally assumed a uniform hygroscopicity value of 5.0×10^{-7} for BC (Ghan et al., 2001; Takemura et al., 2005). Here, the hygroscopicity of hydrophilic BC is set to 0.22 to reflect the enhanced activation capacity of BC particles resulting from the aging process, according to the recommended value reported by Wu et al. (2019). S_{max} denotes the maximum supersaturation, which is related to S_{mi}, updraft velocity, heat diffusion, particle moisture and other factors. The vertical velocity *w* is composed of the grid mean value $\bar{w}$ and the subgrid-scale vertical velocity σ_w, shown as Jiang and Cotton (2005):

$$w = \bar{w} + c \times \sigma_w, \tag{8}$$

where the coefficient *c* is derived from Wang and Penner (2009). The subgrid-scale variability of cloud-base updraft velocity, represented by σ_w, is parameterized from turbulent kinetic energy (TKE) which is calculated online in RegCM-Chem (Lohmann et al., 1999; Virtanen et al., 2025). The effective radius of the cloud droplets R_{eff} can be obtained via the following scheme (Martin et al., 1994):

$$R_{eff} = k\left(\frac{3q}{4\pi\rho_w N_d}\right)^{\frac{1}{3}}, \tag{9}$$

$$k = \frac{(1+2\varepsilon^2)^{\frac{2}{3}}}{(1+\varepsilon^2)^{\frac{1}{3}}}, \tag{10}$$

$$\varepsilon = -12.3 D_{vc}^{-2.20} + 0.41, \tag{11}$$

where q and ρ_w are the cloud liquid water content and water density, respectively. k is the ratio of R_{eff} to the mean volume radius, which is related to the relative dispersion of the cloud size distribution ε (Liu and Daum, 2002). As defined in Eq. (11), a double-parameter scheme for ε proposed by (Zou et al., 2022) is employed here, in which the mean diameter of cloud droplets D_{vc} is expressed as a function of q and N_d.

The autoconversion rate of cloud water to rainwater (*P*) is further introduced in the model to account for the aerosol second indirect effect, as described below (Liou and Ou, 1989; Boucher and Lohmann, 1995):

$$P = C_{l,aut} q^2 \frac{\rho_a}{\rho_w}\left(q N_d \frac{\rho_a}{\rho_w}\right)^{\frac{1}{3}} H(r_e - r_{ec}), \tag{12}$$

where $C_{l,aut}$, ρ_a and $H(r_e - r_{ec})$ are the Stokes constant, air density and Heaviside function, respectively. Details can also be found in Wang et al. (2015) and Zhuang et al. (2025).

2.4 Experimental design

As shown in Fig. 1, the simulated domain is centered at (106°E, 30°N) and covers most regions of East Asia, South Asia and Southeast Asia, with a horizontal resolution of 60 km and grid number of 117 × 137. There are 18 σ-coordinate layers in the vertical direction from the surface to 5 hPa. The 6-h European Centre for Medium-Range Weather Forecasts Re-Analysis-Interim data with a spatial resolution of 1.5° (EIN15) and the weekly mean product of the National Ocean and Atmosphere Administration's Optimum Interpolated sea surface temperature with a spatial resolution of 1° (OISST) are used to drive RegCM-Chem. The chemical data from the Model for Ozone and Related Chemical Tracers, version 4 (MOZART-4) are applied for the initial and boundary conditions of aerosols (Emmons et al., 2010). Anthropogenic emissions are provided by the Multi-resolution Emission Inventory for China (MEIC), a bottom-up emission inventory model developed by

https://doi.org/10.5194/egusphere-2026-2776
Preprint. Discussion started: 15 June 2026

Tsinghua University (Li et al., 2017a; Zheng et al., 2018).

To investigate the impact of dynamic aging scheme on the BC climate effect, eight experiments are carried out in this study (Table 1). Exp. 1 serves as a control run with the fixed aging timescale of 1.15 days and excludes any BC effects. Exps. 2–4 are sensitivity experiments under the same configuration but incorporate BC–radiation interactions, BC–cloud interactions and BC–radiation–cloud interactions, respectively. Therefore, Exps. 2–4 minus Exp. 1 represent the direct (Def_Dir), indirect (Def_Ind) and total (Def_Tot) climate effects of BC under default aging settings, respectively. Exps. 5–8 follow the same design as Exps. 1–4 but replace τ_0 with the dynamic aging scheme to simulate the BC direct (Dyn_Dir), indirect (Dyn_Ind) and total (Dyn_Tot) effects. All simulations are integrated from November 2007 to November 2021, with a spin-up period of one month. Only the outputs in summer (June–August) are analyzed in the following sections. A Student's *t*-test is performed on the seasonal summer means of each year to evaluate the statistical significance of the difference between the experiment results.

Table 1. Numerical experimental setup in this study

Experiment	Aging timescale	BC–radiation interaction	BC–cloud interaction
Exp. 1	1.15 days	off	off
Exp. 2	1.15 days	on	off
Exp. 3	1.15 days	off	on
Exp. 4	1.15 days	on	on
Exp. 5	τ_{mix}	off	off
Exp. 6	τ_{mix}	on	off
Exp. 7	τ_{mix}	off	on
Exp. 8	τ_{mix}	on	on

3. Result

3.1 Model validation

The RegCM-Chem model has been demonstrated to effectively capture the climatic and pollutant characteristics over East Asia (Sun et al., 2012; Zhou et al., 2014; Zhuang et al., 2018b; Gao et al., 2022; Ma et al., 2023; Chen et al., 2024). In this study, we further evaluate the summer output from the Exp. 8 against multiple reference datasets. Specifically, the simulated seasonal mean thermodynamic fields and humidity at 850 and 500 hPa are compared with ERA5 reanalysis data, and surface precipitation is compared with satellite observations from GPM, as shown in Fig. 1. The results indicate that RegCM-Chem successfully reproduces the regional climatic features of East Asia in summer. Additionally, the model's performance in simulating cloud fraction, cloud optical depth and net longwave and shortwave radiative fluxes has been validated in previous studies (Ma et al., 2023; Hu et al., 2024). Figure 1g and h further shows that RegCM-Chem also captures the spatial distribution of BC AOD over East Asia. Although the implementation of the dynamic aging scheme increases AOD values over highly polluted regions in eastern China (as discussed in subsequent sections), the model still tends to underestimate the optical contribution of BC. This bias may be partly attributed to the model's underestimation of BC surface concentrations, as evidenced by comparisons with observations from the China BC Observational Network (Fig. S1 and Table

https://doi.org/10.5194/egusphere-2026-2776
Preprint. Discussion started: 15 June 2026

S1), despite its reasonable reproduction of the BC spatial distribution over China (R=0.69). Such a discrepancy is consistent with findings from most current climate modeling studies, which typically report underestimations of 30–60% in BC surface concentrations across China (Li et al., 2016; Yang et al., 2017; Fang et al., 2020; Liu et al., 2022). While the aging scheme improves the simulation of the decreasing trend in BC concentration to some extent, its effect on reducing the low bias in surface concentrations remains limited, in agreement with the findings of Ghosh et al. (2021) and Shen et al. (2023). This bias may stem from other processes in the climate model, such as grid resolution, dry and wet deposition, and aerosol transport (Wang et al., 2013; Liu et al., 2016). Beyond the systematic comparison, the model-simulated BC loadings also show reasonable agreement with observations with several intensive monitoring sites (Zhou et al., 2024; Tiwari et al., 2025).

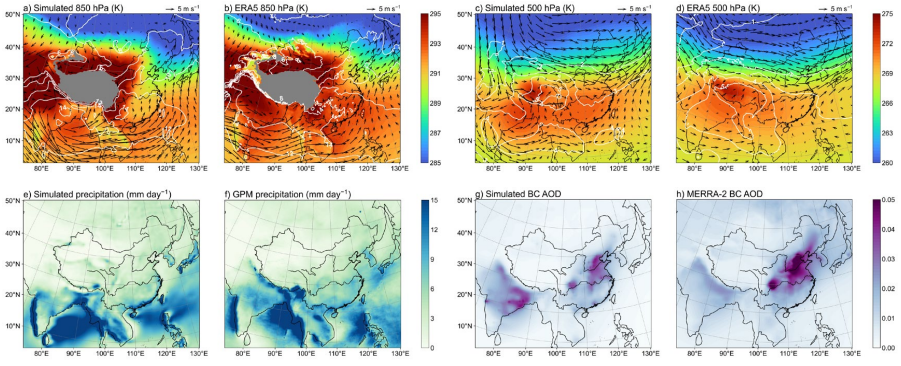

Figure 1. Comparisons between RegCM-Chem summer outputs in the Exp. 8 and multiple reference datasets, including air temperature (shaded, K), specific humidity (contours, g kg^{-1}), wind (vectors, m s^{-1}) at 850 hPa (a and b) and 500 hPa (c and d), precipitation (e and f, mm day^{-1}) and BC aerosol optical depth (AOD) (g and h)

3.2 BC aging timescale

Figure 2a presents the spatial distribution of aerosol precursor (SO_2 + BC + OC) emissions across East Asia from 2008 to 2020. In summer, high emissions are predominantly concentrated in northern India, central to northern and southeastern China, the Pearl River Delta and the Yangtze River Delta. These hotpots, driven primarily by power plants and industrial activities (Li et al., 2017b; Zhuang et al., 2019), exhibit peak emission flux of 4.54 μg m^{-2} s^{-1}. Moreover, except for the Qinghai-Tibet region and northeastern China, the simulated BC aging timescale for the Exp. 8 in most of the eastern China and Indian landmass is generally shorter than the default value used in the model (27.6 hours), which indicates that the fast aging exists widely in summer (Fig. 2b). Even shorter timescales (<10 hours) are observed over the North China Plain and the Sichuan Basin, with the minimum monthly mean reaching 2.84 hours. Under the new dynamic aging scheme, the BC aging timescale exhibits a clear inverse relationship with local pollutant emissions in its spatial distribution, which is attributable to the fact that the abundant condensable species and hygroscopic particles in highly polluter environment accelerate the conversion of fresh BC by enhancing the condensation and coagulation processes. Conversely, in remote regions such as the Qinghai-Tibet region or over the oceanic areas, where anthropogenic emissions are weak and condensable material is limited, BC

https://doi.org/10.5194/egusphere-2026-2776
Preprint. Discussion started: 15 June 2026

aging typically requires more than one day and may even extend to several days.

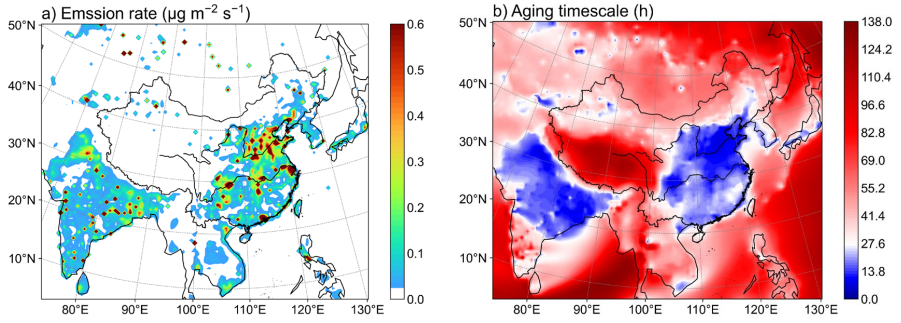

Figure 2. Spatial distribution of the aerosol precursor (SO_2 + OC + BC) emission rate (a, μg m^{-2} s^{-1}) and BC aging timescale (b, h) over East Asia in summer during 2008–2020 in the Exp. 8.

The BC aging timescale simulated in this study is broadly comparable to observations and other modeling studies. Using an environmental chamber approach, Peng et al. (2016) derived a BC aging timescale of 4.6 hours during August–October in Beijing, one of the most polluted areas over East Asia. Similarly, this short timescale was also reported in Shen et al. (2023) (3.8 hours) and Chen et al. (2017) (<2 hours). By comparison, the summertime timescale in our study is found to be 6.94 hours. This overestimation may stem from a sampling bias toward daytime or afternoon periods in these studies, whereas BC aging typically exhibits significant diurnal variation and tends to be slower at night (Riemer et al., 2004; Jacobson, 2010; Chen et al., 2017). Based on constrains from the HIAPER Pole-to-Pole Observations (HIPPO) observations, the *e*-folding timescale of BC emissions from East Asia or near source regions was estimated to be on the order of a few hours (Shen et al., 2014; Zhang et al., 2015; He et al., 2016), consistent with our simulated results (Fig. 2b). By coupling a parameterization scheme of BC aging into the model, Ghosh et al. (2021) and Shen et al. (2023) both indicated that BC aging in western China and the Qinghai-Tibet region occurs on timescales of several days, which are substantially longer than those in eastern China. Overall, the results in this study can be considered to be reasonable in representing BC aging under different atmospheric conditions.

3.3 BC spatial distribution

The summertime spatial distributions of BC surface concentration and column burden under the dynamic aging scheme are presented in Fig. 3a and b. Driven by anthropogenic emissions, high BC levels are mainly found over northern India and eastern China, where the maximum concentration and burden reach 8.82 μg m^{-3} and 2.73 mg m^{-2}, respectively. This spatial pattern is consistent with previous studies (Li et al., 2017c; Zhuang et al., 2019). Northeastern India and the Sichuan Basin exhibit a higher column burden, and this slight discrepancy from the emission distribution may be attributed to topography, atmospheric transport and circulation background (Ji et al., 2015; Yang et al., 2021; Gao et al., 2024). The response of BC loadings to accelerated aging is also shown in Fig. 3, derived from the differences between Exp. 8 and Exp. 4. BC concentrations increase over the southeastern coast of China and the North China Plain, with the maximum exceeding 0.2 μg m^{-3} when the dynamic aging timescale is used (Fig. 3c). Negative changes are found over central to

https://doi.org/10.5194/egusphere-2026-2776
Preprint. Discussion started: 15 June 2026

southern China. Meanwhile, the BC column burden exhibits a spatially coherent decrease across East Asia by a regional mean of 0.12 mg m^{-2} (Fig. 3d). These findings indicate that introducing the dynamic aging timescale can substantially alter the spatial distribution of BC mass.

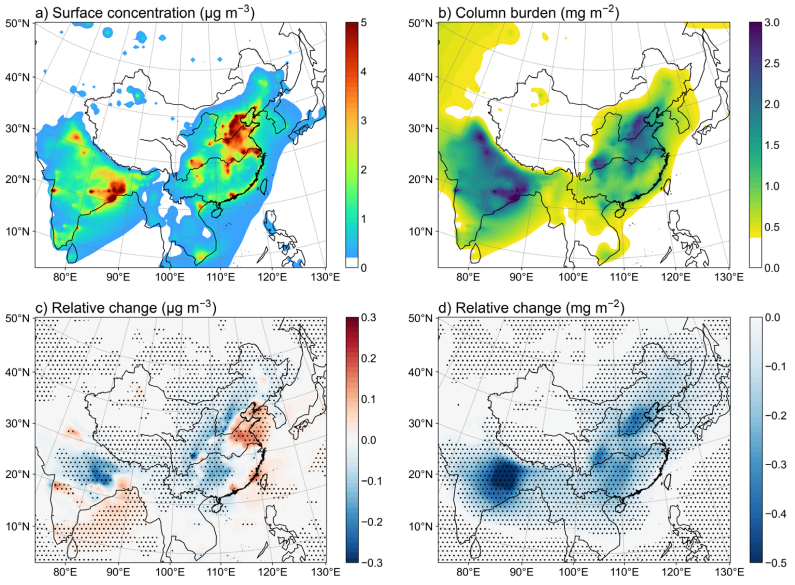

Figure 3. Spatial distribution of the BC surface concentration (a, μg m^{-3}) and column burden (b, mg m^{-2}) over East Asia in summer during 2008–2020 in the Exp. 8. Relative changes in the BC surface concentration (c, μg m^{-3}) and column burden (d, mg m^{-2}) over East Asia in summer during 2008–2020 between the Exp. 8 and Exp. 4. Black-dotted regions denote statistically significant differences at the 90% confidence level based on a Student's *t*-test.

These results can be explained as follows. Generally, rapid BC aging in an area facilitates the conversion of hydrophobic BC to hydrophilic BC (Fig. S2), and vice versa. By altering the partitioning between hydrophobic and hydrophilic particles, changes in the aging rate further alter the removal efficiency and atmospheric lifetime of BC by modulating dry and wet deposition. In regions such as eastern China which undergo faster aging, a larger fraction of hydrophilic BC is involved in both dry and wet deposition, whereas the contribution of hydrophobic particles to deposition is reduced because of their lower abundance (Fig. 4). It is worth noting that, hydrophilic BC is more readily removed by wet deposition but is less susceptible to dry deposition compared with hydrophobic BC. This is attributed to the larger characteristic diameter and higher solubility assigned to hydrophilic tracers, which in turn reduces their dry deposition velocity, consistent with the fundamental principles of aerosol dynamics (Solmon et al., 2006; Ghosh et al., 2021). Therefore, as illustrated in Fig. 4c and f, total BC dry deposition decreases while wet deposition increases, in agreement with the respective changes in hydrophobic and hydrophilic BC. The two processes act in a compensatory manner to co-regulate the overall BC sink. For example, the reduction in dry deposition dominates the increase in surface concentration in the North China Plain, where precipitation and wet deposition are relatively limited in summer (Fig. 3c). A similar phenomenon

https://doi.org/10.5194/egusphere-2026-2776
Preprint. Discussion started: 15 June 2026

observed along the southeastern coastal regions may also be associated with the decreased dry deposition of hydrophobic BC. In terms of vertical distribution, wet deposition, which is dominated by in-cloud scavenging, is the primary mechanism for the removal of BC particles from the atmosphere (Park et al., 2003; Cozic et al., 2007; Ohata et al., 2016). Compared to surface layer, the wet removal efficiency of BC at higher altitudes is more sensitive to the aging rate (Wang et al., 2013; Shen et al., 2023). In the lower troposphere near source regions in eastern China, the high abundance of pollutants still induces rapid aging of BC (Fig. S3). As a result, BC mass is efficiently removed by wet scavenging, leading to an observed decline in the BC column burden (Fig. 3d).

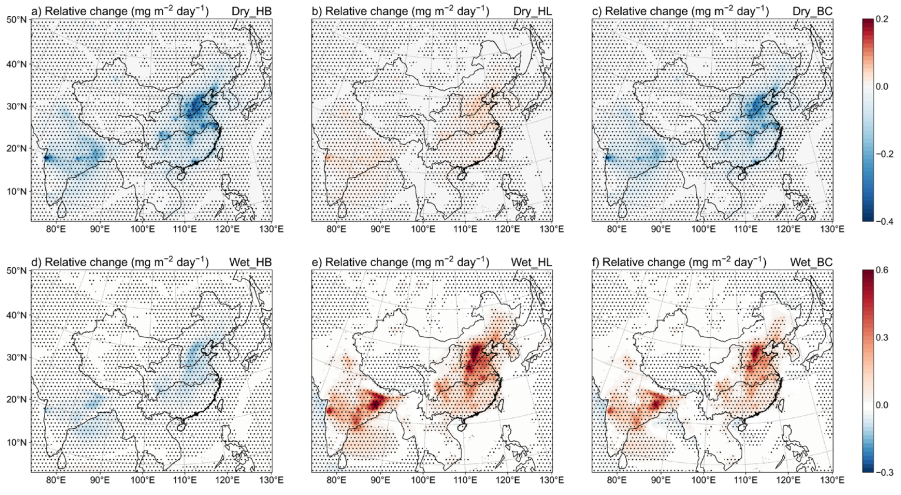

Figure 4. Relative changes in the dry deposition flux (a–c, mg m^{-2} day^{-1}) and wet deposition flux (d–f, mg m^{-2} day^{-1}) of hydrophobic BC (HB, left), hydrophilic BC (HL, center) and total BC (BC, right) over East Asia in summer during 2008–2020 between the Exp. 8 and Exp. 4. Black-dotted regions denote statistically significant differences at the 90% confidence level based on a Student's *t*-test.

3.4 BC direct climate effects

The distributions of the seasonal mean BC aerosol optical depth (AOD) and instantaneous direct radiative forcing (IDRF) for summer are presented in Fig. 5a–c. Consistent with the spatial pattern of BC loadings, high AOD appears in southwestern and central to northern China, with a maximum exceeding 0.05. Owing to the strong absorption of solar radiation, BC can exert a positive IDRF at the top of the atmosphere (TOA) and a negative radiative forcing at the surface. Here, IDRF is defined as the change in net radiative flux under clear-sky conditions caused only by aerosol–radiation interactions, without considering the influences of cloud cover or climate feedbacks. In the IDRF calculation, the radiative transfer model is called twice that with and without BC at each time step. Therefore, the distribution of BC IDRF is closely related to AOD. Generally, the IDRF at the surface exhibits a spatial pattern similar to that at the TOA but a greater magnitude over East Asia, with regional mean values of +0.82 and −3.00 W m^{-2}, respectively. In northwestern and northeastern China where the AOD is low, BC still induce a stronger IDRF at the TOA (Fig. 5b). This is likely because the higher surface albedo in these regions reflects more incoming solar

https://doi.org/10.5194/egusphere-2026-2776
Preprint. Discussion started: 15 June 2026

radiation back into the atmosphere, thereby enhancing BC absorption and leading to a stronger TOA IDRF but weaker surface values (Ocko et al., 2012; Zhuang et al., 2014; Gao et al., 2024).

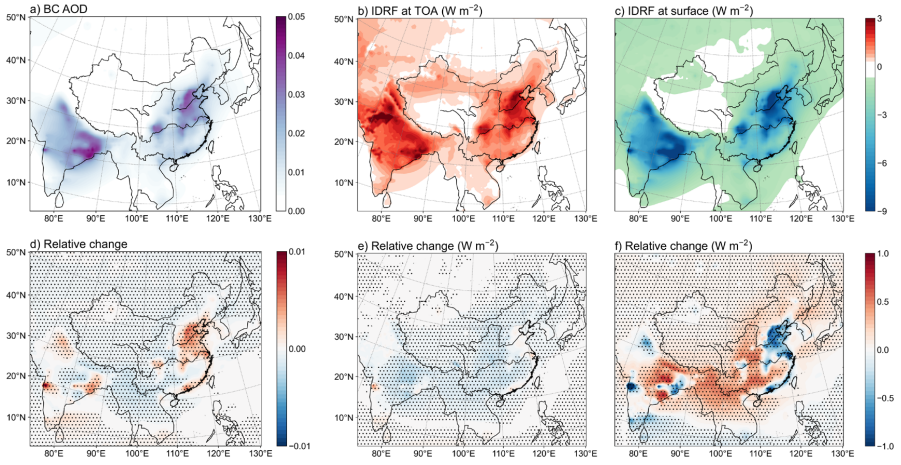

Figure 5. Spatial distribution of the BC aerosol optical depth (AOD) (a), instantaneous direct radiative forcing (IDRF) at the TOA and surface (b and c, W m^{-2}) over East Asia in summer during 2008–2020 in the Dyn_Dir experiment. Relative changes in the BC AOD (d), IDRF at the TOA and surface (e and f, W m^{-2}) over East Asia in summer during 2008–2020 between the Dyn_Dir and Def_Dir experiments. Black-dotted regions denote statistically significant differences at the 90% confidence level based on a Student's *t*-test.

The response of BC AOD to dynamic aging does not remain consistent with the change in column burden, but instead shows a significant increase over eastern China (Fig. 5d). Although AOD represents the vertical integral of total extinction in the atmospheric column, the increase in near-surface BC concentration plays a dominant role in enhanced BC AOD, as BC is primarily concentrated in the lower troposphere. In addition, rapid aging accelerates the production of hydrophilic BC, whose extinction coefficient is larger than that of hydrophobic particles (Solmon et al., 2006), therefore making an additional positive contribution to AOD. This also helps explain why the magnitude of the AOD increase exceeds that of the surface concentration (Figs. 3c and 5d). As a result, in regions where AOD increases, the attenuation of solar radiation by BC is correspondingly strengthened, leading to stronger IDRF at both the TOA and surface (Fig. 5e and f). The sensitivity of surface IDRF in response to AOD is more pronounced, especially in summer when the solar altitude angel is higher (Zhuang et al., 2014).

Radiative perturbations caused by BC can significantly trigger dynamical adjustments. Figure 6 illustrates the changes in horizontal and vertical atmospheric circulation directions driven by the BC direct effects. Adjustments in the low-tropospheric wind field subsequently modulate moisture transport and cloud formation. A comparison between the Dyn_Dir and Def_Dir experiments reveals that the introduction of the dynamic aging scheme dominates this response over eastern China. As shown in Fig. 6c, pronounced southerly wind anomalies originating from the ocean are observed along the southeastern coast of China. A similar feature was also reported by Zhuang et al.

https://doi.org/10.5194/egusphere-2026-2776
Preprint. Discussion started: 15 June 2026

(2019), who suggested that the southerly anomaly could become more substantial in southern China if there were considerable BC loadings in East Asia. This anomaly promotes a cyclonic anomaly near 850 hPa over southern China and effectively transports warm and moist air from the South China Sea inland (Fig. 6a). Meanwhile, the increase in BC-induced heating due to the dynamic aging scheme further strengthens the anomalous ascending motion and meridional circulation, with the shortwave heating wave exceeding 1.4×10^{-6} K s^{-1} (~0.12 K day^{-1}) (Figs. 5d and 6d). These processes collectively promote moisture convergence and a 1–2% increase in cloud fraction (CF) over the southern region. Similarly, moist oceanic airflow and cyclonic updraft are conducive to the increased cloud cover over eastern India and the Indochina Peninsula (Fig. 6a). The responses of the wind field near 850 hPa to the BC direct effects can be advantageous to the development of the East Asian summer monsoon, consistent with previous studies (Wang et al., 2015; Zhuang et al., 2018b; Chen et al., 2020). Over northern China, the BC heating center is located near 35°N, which likewise induces upward motion with the moist accumulation in the middle troposphere. Conversely, compensating subsidence develops in the lower troposphere on both sides of this ascending center, accompanied by decreased specific humidity. (Fig. 6b and d). Horizontally, the southwesterly anomalies formed over the North China Plain under the dynamic aging scheme favor the eastward transport of local moisture, while the compensating northerly flow brings colder and drier air southward from higher latitudes (Fig. 6c), leading to a reduction in CF of 2–3%. Additionally, the stronger semi-direct effect by high BC loadings in northern China also contributes to the suppression of cloud formation to a certain extent (Zhuang et al., 2013).

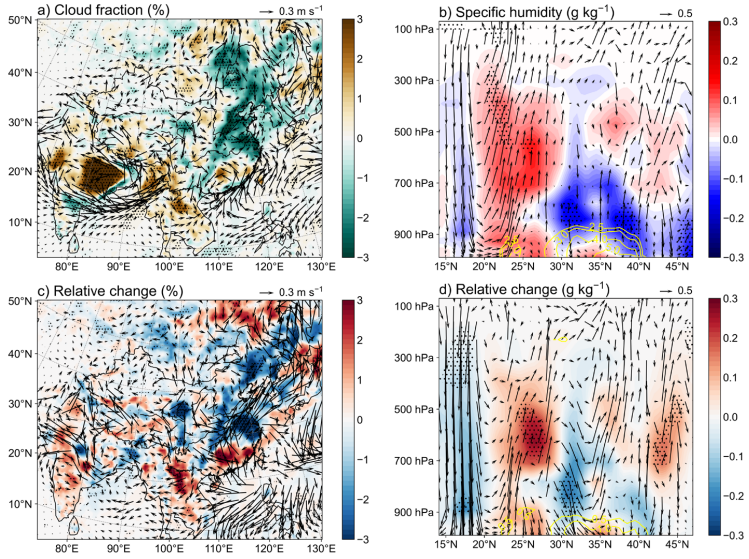

Figure 6. Changes in the (a) wind field (arrow, m s^{-1}) and cloud fraction (shaded, %) near 850 hPa, (b) meridional circulation (arrow), specific humidity (shaded, g kg^{-1}) and shortwave heating rate (contour, 10^{-6} K s^{-1}) in the altitude–longitude section averaged from 112° to 122°E from the BC–radiation interaction over East China in summer during 2008–2020 in the Dyn_Dir experiment. Relative changes in the (c) wind field (arrow, m s^{-1}) and cloud fraction (shaded, %) near 850 hPa, (d) meridional circulation (arrow), specific humidity (shaded, g kg^{-1}) and shortwave heating rate

https://doi.org/10.5194/egusphere-2026-2776
Preprint. Discussion started: 15 June 2026

(contour, 10^{-6} K s^{-1}) in the altitude–latitude section averaged from 112° to 122°E from the BC–radiation interaction over East China in summer during 2008–2020 between the Dyn_Dir and Def_Dir experiments. Black-dotted regions denote statistically significant differences at the 90% confidence level based on a Student's *t*-test.

3.5 BC indirect climate effects

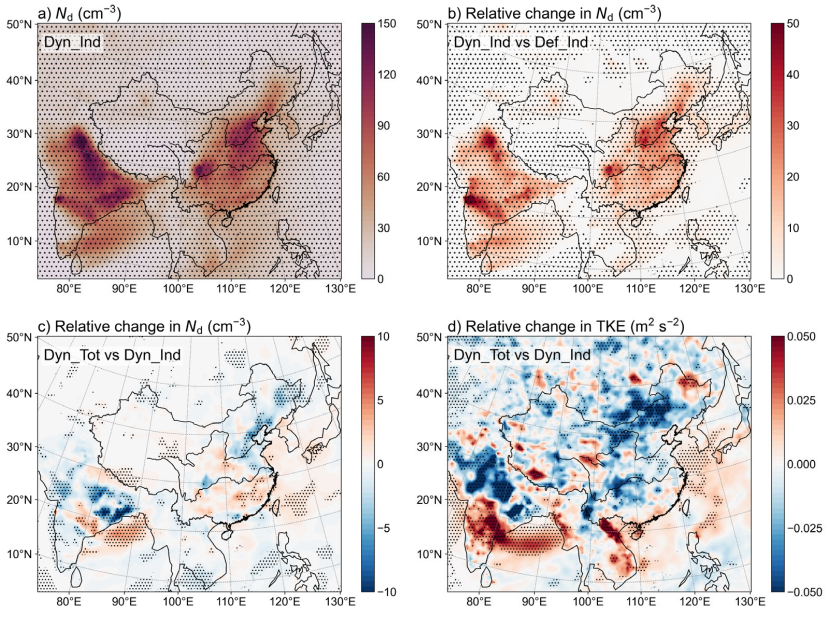

Figure 7. Changes in the cloud droplet number concentration (N_d) (a, cm^{-3}) near 850 hPa from the BC–cloud interaction over East China in summer during 2008–2020 in the Dyn_Ind experiment. Relative changes in the N_d (b, cm^{-3}) near 850 hPa from the BC–cloud interaction over East China in summer during 2008–2020 between the Dyn_Ind and Def_Ind experiments. Relative changes in the N_d (c, cm^{-3}) and TKE (d, m^2 s^{-2}) near 850 hPa from the BC–cloud interaction over East China in summer during 2008–2020 between the Dyn_Tot and Dyn_Ind experiments. Black-dotted regions denote statistically significant differences at the 90% confidence level based on a Student's *t*-test.

Figure 7 presents the changes in the cloud droplet number concentration (N_d) resulting from the BC indirect effects (Dyn_Ind), as well as the changes attributable to the dynamic aging scheme (calculated as Dyn_Ind minus Def_Ind) and the BC direct effects (calculated as Dyn_Tot minus Dyn_Ind). As other aerosols are not considered, the results here only represent the ideal conditions against the background of a clean atmosphere. There is a substantial increase (more than 150 cm^{-3}) in the region with high BC loadings since N_d highly depends on the aerosol number concentration (Fig. 7a). The mean N_d in the lower troposphere is increased by approximately 36.98 cm^{-3} in East Asia for BC. Marked N_d responses are also found over some low-to-mid latitude oceans and remote clean regions, such as the South China Sea and eastern Kazakhstan. This phenomenon may be due

https://doi.org/10.5194/egusphere-2026-2776
Preprint. Discussion started: 15 June 2026

to the abundant water vapor and strong upward convective motions in these regions, which are more favorable for offering higher maximum supersaturation. Moreover, the lower background aerosol concentration weakens the competition for water vapor among particles, thereby increasing the sensitivity of N_d to aerosol perturbations (Reutter et al., 2009; Sullivan et al., 2016; Gryspeerdt et al., 2023). Compared to the default aging scheme, the introduction of the dynamic aging timescale accelerates the production of hydrophilic BC, whose larger hygroscopicity lowers the critical supersaturation and thus increases the potential to be activated as cloud droplets (Mcfiggans et al., 2006; Petters and Kreidenweis, 2007). Consequently, the rapid aging process increases the mean N_d over East Asia by 9.37 cm^{-3}. In the Dyn_Tot experiment, N_d also increases over southern China and Shaanxi Province (Fig. 7c), likely because the upward motion caused by the BC direct heating promotes particle activation (Reutter et al., 2009). This is reflected in the distribution of turbulent kinetic energy (TKE) shown in Fig. 7d, given that the updraft velocity at the cloud base is not explicitly resolved in climate models but instead parameterized from TKE (Virtanen et al., 2025).

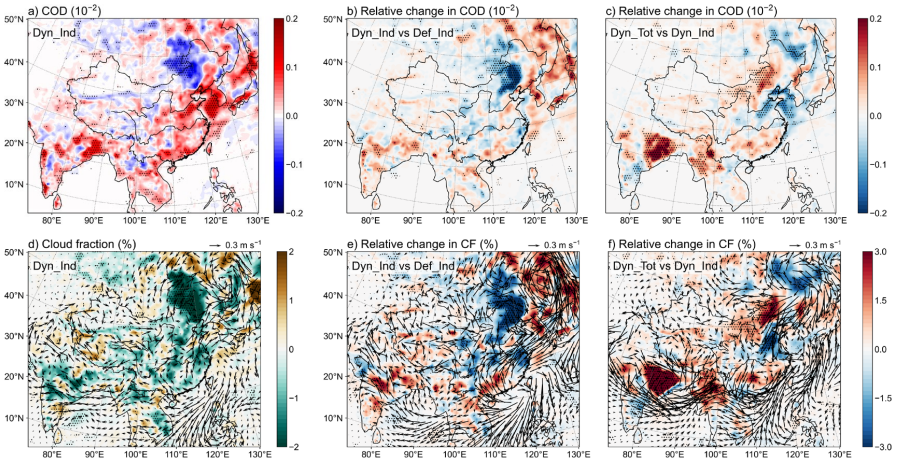

Figure 8. Changes in the cloud optical depth (COD) (a) and cloud fraction (CF) (b, %) near 850 hPa from the BC–cloud interaction over East China in summer during 2008–2020 in the Dyn_Ind experiment. Relative changes in COD (b) and CF (e, %) near 850 hPa from the BC–cloud interaction over East China in summer during 2008–2020 between the Dyn_Ind and Def_Ind experiments. Relative changes in the COD (b) and CF (e, %) near 850 hPa from the BC–cloud interaction over East China in summer during 2008–2020 between the Dyn_Tot and Dyn_Ind experiments. Black-dotted regions denote statistically significant differences at the 90% confidence level based on a Student's *t*-test.

Aerosol particles can reduce the effective radius of cloud droplets by increasing N_d, thereby enhancing both the cloud optical depth (COD) and cloud albedo (Twomey, 1977). In summer, the BC indirect effects lead to a decrease in cloud effective radius (up to −0.9 μm) in the lower troposphere (not shown), accompanied by an overall increase in COD over East Asia (Fig. 8a). However, in addition to the influence of aerosol–cloud interactions on microphysical processes, thermodynamic adjustments induced by the BC indirect effects can also substantially affect cloud formation. In contrast to the BC direct heating, the COD enhancement caused by BC indirect effects

https://doi.org/10.5194/egusphere-2026-2776
Preprint. Discussion started: 15 June 2026

reduces the solar radiation reaching the surface, thereby inducing radiative cooling. This cooling may weaken the development of the East and South Asian Summer Monsoons by diminishing the land-sea thermal gradient (Wang et al., 2015), which in turn suppresses the moisture transport from the oceans, as illustrated in Fig. 8d. Furthermore, the anticyclonic anomaly over southern China contributes to a localized reduction in CF. Consistent but stronger divergence anomalies appear over northeastern China, and their influence exceeds that of the aerosol indirect effects themselves on COD because of the lower N_d there, resulting instead in a decrease in CF and COD. Overall, the thermodynamic responses to BC–cloud interactions are unfavorable for cloud formation over East Asia. A similar pattern is observed in the comparison between the Dyn_Ind and Def_Ind experiments. Although the introduction of the new aging scheme generally leads to a nearly linear increase in N_d over East Asia (Fig. 7b), the response of the atmospheric circulation dominates the differences in cloud cover and COD between the two experiments, even though the increased N_d in still makes a positive contribution to COD to some extent (Fig. 8b and e). Figure 8f reveals the changes in the wind field driven by the BC direct effects similar to those in the Dyn_Dir experiment (Fig. 6a). However, due to the consideration of feedbacks from the BC–cloud interactions, cloud cover in northern or southern China exhibits a stronger response (ranging from −4.13 to 3.71%), which is likely related to BC-induced changes in cloud microphysical processes there. For example, the cyclonic updraft over southern China favors an increase in N_d and cloud formation.

Table 2. Regional means of BC ERF at the TOA and surface, as well as the climate responses in the six experiments.

Variable	Region	Def_Dir	Def_Ind	Def_Tot	Dyn_Dir	Dyn_Ind	Dyn_Tot
TOA ERF (W m^{-2})	NC	4.71×10^{0}	-4.69×10^{0}	1.98×10^{0}	7.91×10^{0}	-1.93×10^{0}	4.56×10^{0}
	SC	3.62×10^{0}	-1.39×10^{0}	1.87×10^{0}	3.90×10^{0}	-7.02×10^{-1}	1.51×10^{0}
	EA	2.31×10^{0}	-1.63×10^{0}	8.20×10^{-1}	3.60×10^{0}	-5.77×10^{-1}	9.01×10^{-1}
Surface ERF (W m^{-2})	NC	-3.27×10^{0}	-3.69×10^{0}	-5.46×10^{0}	-3.26×10^{-1}	-1.22×10^{0}	-3.36×10^{0}
	SC	-1.60×10^{0}	-8.92×10^{-1}	-3.03×10^{0}	-9.68×10^{-1}	-4.11×10^{-1}	-3.14×10^{0}
	EA	-1.58×10^{0}	-1.21×10^{0}	-2.83×10^{0}	-3.14×10^{-1}	-3.62×10^{-1}	-2.68×10^{0}
T_{2m} (K)	NC	-9.30×10^{-2}	-7.65×10^{-2}	-3.45×10^{-2}	9.42×10^{-2}	-1.79×10^{-3}	4.42×10^{-2}
	SC	-1.63×10^{-2}	-3.89×10^{-2}	-4.69×10^{-2}	-3.95×10^{-3}	-1.08×10^{-2}	-4.22×10^{-2}
	EA	-6.42×10^{-2}	-7.07×10^{-2}	-5.99×10^{-2}	2.85×10^{-2}	1.00×10^{-2}	-3.73×10^{-2}
Precipitation (mm/day)	NC	-1.30×10^{-1}	-5.40×10^{-2}	-1.45×10^{-1}	-1.08×10^{-2}	-1.45×10^{-1}	-9.17×10^{-2}
	SC	7.45×10^{-2}	7.48×10^{-3}	1.30×10^{-1}	1.69×10^{-1}	-9.63×10^{-2}	1.33×10^{-1}

https://doi.org/10.5194/egusphere-2026-2776
Preprint. Discussion started: 15 June 2026

	EA	1.06 × 10^{-1}	7.94 × 10^{-2}	4.99 × 10^{-2}	7.36 × 10^{-2}	−1.13 × 10^{-1}	6.35 × 10^{-2}

NC: northern China (30°–40°N, 110°–120°E)
SC: southern China (22°–30°N, 100°–120°E)
EA: East Asia (20°–45°N, 100°–130°E)

3.6 BC effective radiative forcing and regional climate responses

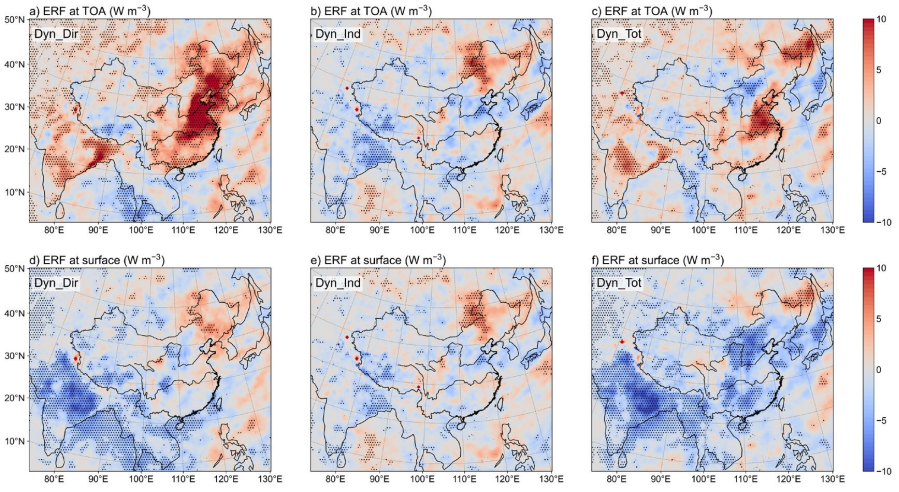

Figure 9. Spatial distribution of the BC effective radiative forcing (ERF) at the TOA and surface (a–c and d–f, W m^{-2}) over East Asia in summer during 2008–2020 in the Dyn_Dir (left), Dyn_Ind (center) and Dyn_Tot (right) experiments. Black-dotted regions denote statistically significant differences at the 90% confidence level based on a Student's *t*-test.

Since the Fifth Assessment Report of the Intergovernmental Panel on Climate Change, effective radiative forcing (ERF) has gained more attention because the climate response to aerosols can also influence the energy balance of the Earth–atmosphere system (IPCC, 2013). Unlike IDRF, ERF is defined as the changes in net radiative flux at the TOA and surface after a perturbation is imposed, allowing for the rapid adjustments of meteorological factors in the troposphere and stratosphere. In this study, the summer ERFs induced by BC–radiation interactions (ERF_{bri}), BC–cloud interactions (ERF_{bci}) and BC–radiation–cloud interactions (total ERF) under the new aging scheme are calculated as the differences between the corresponding sensitivity experiments and the control experiment, as described in the Method section (Fig. 9). Similar to the spatial patterns of BC IDRF, the ERF_{bri} over most of the study domain is positive at the TOA and negative at the surface due to the strong absorption of solar radiation, with regional mean values of +3.60 and −0.31 W m^{-2} over East Asia in summer, respectively (Fig. 9a and d). However, significant discrepancies exist between IDRF and ERF_{bri} because the latter accounts for meteorological adjustments, primarily driven by cloud responses (Gao et al., 2024). For instance, reduced CF over northern China and the North China Plain allows more solar radiation to be absorbed and to reach the surface (Fig. 6a), thereby enhancing radiative income at both the TOA and surface. Such positive adjustments can offset or

https://doi.org/10.5194/egusphere-2026-2776
Preprint. Discussion started: 15 June 2026

even exceed the initial negative IDRF, leading to a net positive ERF_{bri} at the surface (Fig. 9d). Opposite trends are observed in regions such as India. The significance of climate feedbacks for the ERF_{bri} has also been demonstrated in previous studies, which suggest that approximately 30–50% of the BC IDRF can be affected by adjustments in clouds and the temperature lapse rate (Stjern et al., 2017; Smith et al., 2018; Zhao and Suzuki, 2019). In contrast, the ERF_{bci} exhibits a more consistent spatial distribution at the TOA and at the surface in East Asia (Fig. 9b and e), as the BC indirect effects are primarily mediated through cloud-driven radiative changes. The increase in low-level COD associated with BC-induced N_d enhances the radiative cooling effect of clouds. As a result, the BC indirect effects produce predominantly negative ERF_{bci} at both the TOA and surface over East Asia, with maximum values reaching −7.46 and −5.94 W m^{-2}, respectively. Nevertheless, strong circulation and cloud responses also modulate the spatial distribution of ERF_{bci} in a similar way to some extent. As shown in Figs. 8d and 9, decreased cloud cover in the middle and lower reaches of the Yangtze River and the upper Yellow River results in localized positive ERF_{bci}. Although the sign of the total ERF remains consistent with that of ERF_{bri}, the inclusion of cooling effects from BC–cloud interactions results in a more surface ERF of −2.68 W m^{-2} over East Asia, whereas the total ERF at the TOA is reduced to 0.90 W m^{-2}. In addition, the total ERF is not simply equal to the linear sum of the ERF_{bri} and ERF_{bci}, which may be closely related to climate feedbacks (Zhuang et al., 2019; Chen et al., 2020; Gao et al., 2024). This nonlinear behavior is also evident in the regional differences before and after the introduction of the dynamic aging scheme, as shown in Table 2.

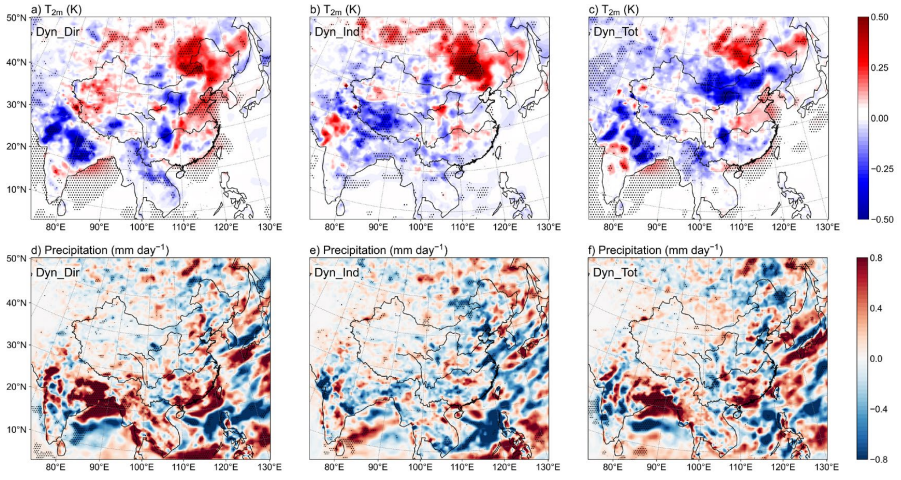

Figure 10. Changes in the surface air temperature at 2 m (T_{2m}) (a–c, K) and precipitation (d–f, mm day^{-1}) over East China in summer during 2008–2020 in the Dyn_Dir (left), Dyn_Ind (center) and Dyn_Tot (right) experiments. Black-dotted regions denote statistically significant differences at the 90% confidence level based on a Student's *t*-test.

Figure 10a–c illustrates the responses of surface air temperature at 2 m to different BC climate effects over East Asia during summer with the new aging scheme. The spatial distribution of the air temperature anomalies aligns closely with the ERF patterns but exhibits an inverse relationship with

https://doi.org/10.5194/egusphere-2026-2776
Preprint. Discussion started: 15 June 2026

cloud cover. In the Dyn_Dir experiment, the reduction in surface radiation directly induces surface cooling over the Sichuan Basin and southern China (Figs. 9d and 10a), with a maximum temperature decrease of −0.54 K. In contrast, surface warming occurs over the North China Plain and northeastern China, where low-level CF decreases and ERF_{bri} becomes positive. A similar relationship is also evident in the temperature changes induced by BC–cloud interactions, with a regional mean anomaly of −0.01 K over eastern China (20°–40°N, 100°–120°E), ranging from −0.27 to 0.35 K (Fig. 10b). Simulation in the Dyn_Tot experiment shows an average warming of 0.044 K in northern China and a cooling of −0.042 K in the south due to the BC total effect. Notably, the temperature changes here further highlight the nonlinearity of regional climate responses (Zhuang et al., 2019). For example, while the increased air temperature is found over northeastern China in both Dyn_Dir and Dyn_Ind experiments, an opposite cooling trend appears in the Dyn_Tot experiment. Feedbacks from wind fields and cloud cover play a critical role in this nonlinearity, further triggering the complex and heterogeneous response of precipitation.

BC–radiation interactions primarily affect precipitation through thermodynamic adjustments by radiative perturbations. Generally, local floods result from an increase in moisture transport or a convergence anomaly, and vice versa (Figs. 6a and 10d). For instance, moisture convergence over southern China leads to a significant increase in precipitation there. Although the BC loading is relatively low in this region, the magnitude of precipitation change exceeds that in northern China. This aligns with previous studies suggesting that circulation responses in regions where AOD is weak dominate precipitation changes (Gu et al., 2016; Chen et al., 2020; Zhuang et al., 2025). Compared with the annual mean (Gao et al., 2024), summer precipitation changes are also substantially larger because of the more vigorous background atmospheric circulation, which also supports this opinion. Similarly, stronger precipitation responses can also be observed over the ocean, where compensating airflows drive more pronounced moisture transport. A widespread reduction in precipitation over East Asia is observed in the Dyn_Ind experiment, with regional mean and maximum values of −0.11 and −1.92 mm day^{-1}, respectively (Fig. 10e). In addition to the aerosol second indirect effect, which suppresses precipitation by reducing the conversion rate of cloud water into rainwater, the influence of large-scale circulation patterns may exceed that of local cloud microphysical processes on seasonal timescales by modulating monsoon intensity and moisture transport pathways (Wang et al., 2021; Wang et al., 2024; Qie et al., 2025). Consequently, precipitation shows an increase over parts of central China. With respect to the total effects, the circulation background dominated by the BC direct effects shapes the evolution of the south–wet and north–dry precipitation patterns in summer, with regional mean values of −0.09 and +0.13 mm day^{-1} in southern and northern China, respectively (Figs. 8f and 10f). The responses in precipitation found in this study agree with some previous findings (Menon et al., 2002; Zhuang et al., 2018b; Gao et al., 2024).

4 Conclusion

This study incorporates a dynamic BC aging parameterization scheme, which explicitly accounts for condensation and coagulation processes, into RegCM-Chem, and systematically investigates the impacts of aging representation on the direct, indirect and total climate effects of BC over East Asia during summer. The simulation results indicate that the BC aging timescale is generally shorter in heavily polluted regions than the conventional fixed e-folding aging timescale of 1.15 days. In

https://doi.org/10.5194/egusphere-2026-2776
Preprint. Discussion started: 15 June 2026

particular, the BC aging process can be completed within 10 hours over the North China Plain and the Sichuan Basin, with the minimum monthly mean reaching 2.84 hours, whereas longer timescales are found in remote regions such as the Tibetan Plateau and oceanic areas. The simulated aging timescales is broadly consistent with previous studies (Peng et al., 2016; Shen et al., 2023; Fierce et al., 2025), which reported BC aging on timescales of several hours in Beijing and other polluted environments, in contrast to much slower aging over clean aeras. The introduction of the dynamic aging scheme substantially alters the spatial distribution and removal pathways of BC. Accelerated aging promotes the formation and wet deposition of hydrophilic BC, leading to a regional mean reduction of 0.12 mg m^{-2} in BC column burden over East Asia. However, localized increases in BC surface concentrations are observed in the North China Plain and southeastern coastal China, primarily driven by the overcompensation associated with the weakened dry deposition near the surface.

While earlier work has primarily focused on the developing the representation of BC aging processes in climate models (Ghosh et al., 2021; Shen et al., 2023), this study extends these efforts by quantifying how the BC climate effects respond to dynamic aging. The enhancement of BC AOD over eastern China is attributed to increases in BC surface concentrations and the greater extinction efficiency of hydrophilic BC, further amplifying the IDRF at both of the TOA and surface under the dynamic aging scheme. This stronger direct heating by BC induces a pronounced circulation adjustment, which is conducive to the development of the East Asian summer monsoon. This process strengthens low-level convergence and ascending motion over southern China, thereby facilitating moisture transport and increasing cloud cover. In contrast, compensating subsidence and the semi-direct effects of BC tend to suppress cloud formation in northern China. Additionally, dynamic aging accelerates the production of hydrophilic BC and its participation in N_d formation in the lower troposphere, resulting in a significant cloud radiative cooling effect through the increased COD. However, the dynamic adjustments in atmospheric circulation may outweigh the influence of cloud microphysical processes, thereby playing a dominant role in determining cloud responses in certain regions (Zhuang et al., 2025).

Our study further investigates the BC ERF and regional climate responses under the dynamic scheme. BC–radiation interactions exert a positive ERF at the TOA and a negative ERF at the surface, with regional means over East Asia of +3.60 and −0.31 W m^{-2}, respectively. The signs of total ERF at both the TOA and surface are generally consistent with those of the direct effect but with the more negative magnitudes (+0.90 and −2.68 W m^{-2}) due to the cooling contribution from aerosol–cloud interactions. Similar to the ERF, adjustments in atmospheric circulation and cloud cover intensify the nonlinear responses of regional climate, indicating that the total climate effect is not a simple linear superposition of direct and indirect effects. In terms of the BC total climate effects, the circulation background dominated by BC–radiation interactions shapes a characteristic "southern flooding and northern drought" precipitation pattern in summer, with the regional mean anomalies of +0.13 and −0.09 mm day^{-1} over southern and northern China, respectively. The responses in precipitation found in this study agree with some recent study (Zhuang et al., 2018b; Gao et al., 2024). Meanwhile, BC can lead to slight warming in northern China and cooling in the south.

https://doi.org/10.5194/egusphere-2026-2776
Preprint. Discussion started: 15 June 2026

There are a few limitations that should be addressed in the future. First, although the simulated BC aging timescales are broadly comparable to most modeling estimates, direct observational evidence for BC aging timescales and column burden remain limited. Second, the introduction of the dynamic aging scheme does not fully solve the pre-existing underestimation of BC surface concentrations and optical contribution, suggesting that uncertainties in other processes such as emissions, transport and grid resolution may still affect estimates of BC loadings and climate effects (Wang et al., 2013; Liu et al., 2016). Third, the improved representation of BC aging in this study focused on the aging timescale. Future developments should further incorporate observational constraints on BC size distributions, mixing state, coating properties and absorption enhancement (Liu et al., 2024; Guan et al., 2026a; Liu et al., 2026). Despite these limitations, these findings highlight that the representation of BC aging in the regional climate model is crucial for more reliable assessments of aerosol radiative forcing and regional climate effects, particularly in highly polluted and monsoon-dominated regions, which improves the understanding of aerosol–climate interactions in East Asia.

https://doi.org/10.5194/egusphere-2026-2776
Preprint. Discussion started: 15 June 2026

Code and data availability

The source codes and input data of RegCM-Chem, including the EIN15 data, the OISST data and the MOZART-4 data can be downed from http://clima-dods.ictp.it/data/regcm4/. The MEIC anthropogenic emission inventories are available at http://www.meicmodel.org. The ERA5 data are publicly available from https://cds.climate.copernicus.eu/datasets. The MERRA-2 and GPM data are available via GES DISC at https://disc.gsfc.nasa.gov/datasets.

Author contribution

BZ designed the study and carried out the simulation. PG preformed the analysis and drafted the manuscript. All authors helped to review and edit this manuscript.

Competing interests

The contact author has declared that none of the authors has any competing interests.

Acknowledgements

We greatly thank Wenxiang Shen for providing the BC concentration data from the China BC Observational Network. We also thank all the scientists, software engineers and administrators who contributed to the development of RegCM-Chem.

Financial support

This work was supported by the National Key R&D Program of China, the National Natural Science Foundation of China (2024YFC3711904, 42075099), and the Frontiers Science Center for Critical Earth Material Cycling of Nanjing University.

https://doi.org/10.5194/egusphere-2026-2776
Preprint. Discussion started: 15 June 2026

References

Abdul-Razzak, H. and Ghan, S. J.: A parameterization of aerosol activation 2. Multiple aerosol types, J. Geophys. Res. Atmos., 105, 6837-6844, https://doi.org10.1029/1999jd901161, 2000.

Abdul-Razzak, H. and Ghan, S. J.: A parameterization of aerosol activation - 3. Sectional representation, J. Geophys. Res. Atmos., 107, AAC 1-1-AAC 1-6, https://doi.org10.1029/2001jd000483, 2002.

Bauer, S. E., Wright, D. L., Koch, D., Lewis, E. R., McGraw, R., Chang, L. S., Schwartz, S. E., and Ruedy, R.: MATRIX (Multiconfiguration Aerosol TRacker of mIXing state): an aerosol microphysical module for global atmospheric models, Atmos. Chem. Phys., 8, 6003-6035, https://doi.org10.5194/acp-8-6003-2008, 2008.

Bond, T. C., Doherty, S. J., Fahey, D. W., Forster, P. M., Berntsen, T., DeAngelo, B. J., Flanner, M. G., Ghan, S., Kaercher, B., Koch, D., Kinne, S., Kondo, Y., Quinn, P. K., Sarofim, M. C., Schultz, M. G., Schulz, M., Venkataraman, C., Zhang, H., Zhang, S., Bellouin, N., Guttikunda, S. K., Hopke, P. K., Jacobson, M. Z., Kaiser, J. W., Klimont, Z., Lohmann, U., Schwarz, J. P., Shindell, D., Storelvmo, T., Warren, S. G., and Zender, C. S.: Bounding the role of black carbon in the climate system: A scientific assessment, J. Geophys. Res. Atmos., 118, 5380-5552, https://doi.org10.1002/jgrd.50171, 2013.

Boucher, O. and Lohmann, U.: THE SULFATE-CCN-CLOUD ALBEDO EFFECT - A SENSITIVITY STUDY WITH 2 GENERAL-CIRCULATION MODELS, Tellus Ser. B-Chem. Phys. Meteorol., 47, 281-300, https://doi.org10.1034/j.1600-0889.47.issue3.1.x, 1995.

Cao, H., Zhuang, B., Zhou, Y., Gao, P., Hu, Y., Wang, T., Li, S., Li, M., Xie, M., and Liu, Q.: Impact of boundary layer schemes in RegCM-Chem on East Asian climate and its response to the aerosol-radiation interaction, Atmos. Res., 337, 108951, https://doi.orghttps://doi.org/10.1016/j.atmosres.2026.108951, 2026.

Cappa, C. D., Onasch, T. B., Massoli, P., Worsnop, D. R., Bates, T. S., Cross, E. S., Davidovits, P., Hakala, J., Hayden, K. L., Jobson, B. T., Kolesar, K. R., Lack, D. A., Lerner, B. M., Li, S.-M., Mellon, D., Nuaaman, I., Olfert, J. S., Petaja, T., Quinn, P. K., Song, C., Subramanian, R., Williams, E. J., and Zaveri, R. A.: Radiative Absorption Enhancements Due to the Mixing State of Atmospheric Black Carbon, Science, 337, 1078-1081, https://doi.org10.1126/science.1223447, 2012.

Chakrabarty, R. K. and Heinson, W. R.: Scaling Laws for Light Absorption Enhancement Due to Nonrefractory Coating of Atmospheric Black Carbon Aerosol, Phys. Rev. Lett., 121, https://doi.org10.1103/PhysRevLett.121.218701, 2018.

Chen, H., Zhuang, B., Liu, J., Ma, D., Li, S., Wang, T., Xie, M., and Li, M.: The influence of the black carbon warming effect on near-surface ozone in China in summer, Atmos. Res., 301, 107284, https://doi.orghttps://doi.org/10.1016/j.atmosres.2024.107284, 2024.

Chen, H., Zhuang, B., Liu, J., Li, S., Wang, T., Xie, X., Xie, M., Li, M., and Zhao, M.: Regional Climate Responses in East Asia to the Black Carbon Aerosol Direct Effects from India and China in Summer, J. Clim., 33, 9783-9800, https://doi.org10.1175/jcli-d-19-0706.1, 2020.

Chen, X., Wang, Z., Yu, F., Pan, X., Li, J., Ge, B., Wang, Z., Hu, M., Yang, W., and Chen, H.: Estimation of atmospheric aging time of black carbon particles in the polluted atmosphere over central-eastern China using microphysical process analysis in regional chemical transport model, Atmos. Environ., 163, 44-56, https://doi.org10.1016/j.atmosenv.2017.05.016, 2017.

Chung, S. H. and Seinfeld, J. H.: Global distribution and climate forcing of carbonaceous aerosols, J. Geophys. Res.: Atmos., 107, AAC 14-11-AAC 14-33, https://doi.orghttps://doi.org/10.1029/2001JD001397, 2002.

https://doi.org/10.5194/egusphere-2026-2776
Preprint. Discussion started: 15 June 2026

Cooke, W. F., Liousse, C., Cachier, H., and Feichter, J.: Construction of a 1° x 1° fossil fuel emission data set for carbonaceous aerosol and implementation and radiative impact in the ECHAM4 model, J. Geophys. Res. Atmos., 104, 22137-22162, https://doi.org10.1029/1999jd900187, 1999.

Cozic, J., Verheggen, B., Mertes, S., Connolly, P., Bower, K., Petzold, A., Baltensperger, U., and Weingartner, E.: Scavenging of black carbon in mixed phase clouds at the high alpine site Jungfraujoch, Atmos. Chem. Phys., 7, 1797-1807, https://doi.org10.5194/acp-7-1797-2007, 2007.

Dalirian, M., Ylisirnio, A., Buchholz, A., Schlesinger, D., Strom, J., Virtanen, A., and Riipinen, I.: Cloud droplet activation of black carbon particles coated with organic compounds of varying solubility, Atmos. Chem. Phys., 18, 12477-12489, https://doi.org10.5194/acp-18-12477-2018, 2018.

Denis, B., Laprise, R., Caya, D., and Cote, J.: Downscaling ability of one-way nested regional climate models: the Big-Brother Experiment, Clim. Dyn., 18, 627-646, https://doi.org10.1007/s00382-001-0210-0, 2002.

Ding, A. J., Huang, X., Nie, W., Sun, J. N., Kerminen, V. M., Petaja, T., Su, H., Cheng, Y. F., Yang, X. Q., Wang, M. H., Chi, X. G., Wang, J. P., Virkkula, A., Guo, W. D., Yuan, J., Wang, S. Y., Zhang, R. J., Wu, Y. F., Song, Y., Zhu, T., Zilitinkevich, S., Kulmala, M., and Fu, C. B.: Enhanced haze pollution by black carbon in megacities in China, Geophys. Res. Lett., 43, 2873-2879, https://doi.org10.1002/2016gl067745, 2016.

Dusek, U., Reischl, G. P., and Hitzenberger, R.: CCN activation of pure and coated carbon black particles, Environ. Sci. Technol., 40, 1223-1230, https://doi.org10.1021/es0503478, 2006.

Emmons, L. K., Walters, S., Hess, P. G., Lamarque, J. F., Pfister, G. G., Fillmore, D., Granier, C., Guenther, A., Kinnison, D., Laepple, T., Orlando, J., Tie, X., Tyndall, G., Wiedinmyer, C., Baughcum, S. L., and Kloster, S.: Description and evaluation of the Model for Ozone and Related chemical Tracers, version 4 (MOZART-4), Geosci. Model Dev., 3, 43-67, https://doi.org10.5194/gmd-3-43-2010, 2010.

Fang, C., Zhu, B., Pan, C., Yun, X., Ding, D., and Tao, S.: Regional and Sectoral Sources for Black Carbon Over South China in Spring and Their Sensitivity to East Asian Summer Monsoon Onset, J. Geophys. Res. Atmos., 125, https://doi.org10.1029/2020jd033219, 2020.

Fang, C., Zhu, B., Pan, C., Qian, P., Wang, D., Zhang, Y., Lu, C., and Liao, H.: Inconsistent Fast and Slow Responses of East Asian Summer Monsoon Precipitation Forced by Black Carbon, J. Clim., 38, 1081-1103, https://doi.org10.1175/jcli-d-24-0067.1, 2025.

Fierce, L., Riemer, N., and Bond, T. C.: TOWARD REDUCED REPRESENTATION OF MIXING STATE FOR SIMULATING AEROSOL EFFECTS ON CLIMATE, Bull. Am. Meteorol. Soc., 98, 971-980, https://doi.org10.1175/bams-d-16-0028.1, 2017.

Fierce, L., Li, Y., Feng, Y., Riemer, N., Schutgens, N. A. J., Aiken, A. C., Dubey, M. K., Ma, P.-L., and Wuebbles, D.: Constraining Black Carbon Aging in Global Models to Reflect Timescales for Internal Mixing, J. Adv. Model. Earth Syst., 17, https://doi.org10.1029/2024ms004471, 2025.

Fountoukis, C. and Nenes, A.: ISORROPIA II: a computationally efficient thermodynamic equilibrium model for K^+–$Ca2^+$–$Mg2^+$–$NH4^+$–Na^+–$SO42^-$–$NO3^-$–Cl^-–H2O aerosols, Atmos. Chem. Phys., 7, 4639-4659, https://doi.org10.5194/acp-7-4639-2007, 2007.

Furutani, H., Dall'osto, M., Roberts, G. C., and Prather, K. A.: Assessment of the relative importance of atmospheric aging on CCN activity derived from field observations, Atmos. Environ., 42, 3130-3142, https://doi.org10.1016/j.atmosenv.2007.09.024, 2008.

Gao, P., Gao, Y., Zhou, Y., Cao, H., Hu, Y., Li, S., Liang, S., Wang, T., Xie, M., Li, M., and Zhuang, B.: Changes in the Direct Climate Effect of Black Carbon Aerosols in East Asia Under the "Dual

https://doi.org/10.5194/egusphere-2026-2776
Preprint. Discussion started: 15 June 2026

Carbon" Goal of China, J. Geophys. Res. Atmos., 129, e2024JD040874, https://doi.org10.1029/2024jd040874, 2024.

Gao, Y., Zhuang, B., Wang, T., Chen, H., Li, S., Wei, W., Lin, H., and Li, M.: Climatic-Environmental Effects of Aerosols and Their Sensitivity to Aerosol Mixing States in East Asia in Winter, Remote Sens., 14, https://doi.org10.3390/rs14153539, 2022.

Ghan, S., Laulainen, N., Easter, R., Wagener, R., Nemesure, S., Chapman, E., Zhang, Y., and Leung, R.: Evaluation of aerosol direct radiative forcing in MIRAGE, J. Geophys. Res. Atmos., 106, 5295-5316, https://doi.org10.1029/2000jd900502, 2001.

Ghosh, S., Riemer, N., Giuliani, G., Giorgi, F., Ganguly, D., and Dey, S.: Sensitivity of Carbonaceous Aerosol Properties to the Implementation of a Dynamic Aging Parameterization in the Regional Climate Model RegCM, J. Geophys. Res. Atmos., 126, https://doi.org10.1029/2020jd033613, 2021.

Ghosh, S., Dey, S., Das, S., Riemer, N., Giuliani, G., Ganguly, D., Venkataraman, C., Giorgi, F., Tripathi, S. N., Ramachandran, S., Rajesh, T. A., Gadhavi, H., and Srivastava, A. K.: Towards an improved representation of carbonaceous aerosols over the Indian monsoon region in a regional climate model: RegCM, Geosci. Model Dev., 16, 1-15, https://doi.org10.5194/gmd-16-1-2023, 2023.

Giorgi, F.: A PARTICLE DRY-DEPOSITION PARAMETERIZATION SCHEME FOR USE IN TRACER TRANSPORT MODELS, J. Geophys. Res. Atmos., 91, 9794-9806, https://doi.org10.1029/JD091iD09p09794, 1986.

Giorgi, F.: Two-dimensional simulations of possible mesoscale effects of nuclear war fires: 1. Model description, J. Geophys. Res.: Atmos., 94, 1127-1144, https://doi.orghttps://doi.org/10.1029/JD094iD01p01127, 1989.

Giorgi, F., Coppola, E., Solmon, F., Mariotti, L., Sylla, M. B., Bi, X., Elguindi, N., Diro, G. T., Nair, V., Giuliani, G., Turuncoglu, U. U., Cozzini, S., Guettler, I., O'Brien, T. A., Tawfik, A. B., Shalaby, A., Zakey, A. S., Steiner, A. L., Stordal, F., Sloan, L. C., and Brankovic, C.: RegCM4: model description and preliminary tests over multiple CORDEX domains, Clim. Res., 52, 7-29, https://doi.org10.3354/cr01018, 2012.

Gryspeerdt, E., Povey, A. C., Grainger, R. G., Hasekamp, O., Hsu, N. C., Mulcahy, J. P., Sayer, A. M., and Sorooshian, A.: Uncertainty in aerosol-cloud radiative forcing is driven by clean conditions, Atmos. Chem. Phys., 23, 4115-4122, https://doi.org10.5194/acp-23-4115-2023, 2023.

Gu, Y., Xue, Y., De Sales, F., and Liou, K. N.: A GCM investigation of dust aerosol impact on the regional climate of North Africa and South/East Asia, Clim. Dyn., 46, 2353-2370, https://doi.org10.1007/s00382-015-2706-y, 2016.

Guan, L., Cohen, J. B., Wang, S., Tiwari, P., Liu, Z., and Qin, K.: Improving Aerosol Absorption Estimates Via Size-Resolved Constraints Based on AERONET and In Situ Measurements, Geophys. Res. Lett., 53, https://doi.org10.1029/2025gl117418, 2026a.

Guan, L., Cohen, J. B., Wang, S., Tiwari, P., Liu, Z., Li, Z., and Qin, K.: In-tandem multi-waveband particulate absorption and size observations yield substantial changes in radiative forcing over industrial Central China, Atmos. Chem. Phys., 26, 3107-3123, https://doi.org10.5194/acp-26-3107-2026, 2026b.

He, C., Li, Q., Liou, K.-N., Qi, L., Tao, S., and Schwarz, J. P.: Microphysics-based black carbon aging in a global CTM: constraints from HIPPO observations and implications for global black carbon budget, Atmos. Chem. Phys., 16, 3077-3098, https://doi.org10.5194/acp-16-3077-2016, 2016.

Hu, Y., Zhuang, B., Zhou, Y., Gao, Y., Gao, P., Wang, T., Li, S., Xie, M., and Li, M.: Effects of emission reductions on major anthropogenic aerosol-radiation-cloud interactions in East Asia in winter during

https://doi.org/10.5194/egusphere-2026-2776
Preprint. Discussion started: 15 June 2026

2007-2020, Atmos. Environ., 327, https://doi.org10.1016/j.atmosenv.2024.120499, 2024.

Huang, Y., Chameides, W. L., and Dickinson, R. E.: Direct and indirect effects of anthropogenic aerosols on regional precipitation over east Asia, J. Geophys. Res. Atmos., 112, https://doi.org10.1029/2006jd007114, 2007.

IPCC. Climate Change 2013: The Physical Science Basis. Contribution of Working Group I to the Fifth Assessment Report of the Intergovernmental Panel on Climate Change [Stocker, T.F., D. Qin, G.-K. Plattner, M. Tignor, S.K. Allen, J. Boschung, A. Nauels, Y. Xia, V. Bex and P.M. Midgley (eds.)]. Cambridge University Press, 2013.

IPCC. Climate Change 2021: The Physical Science Basis. Contribution of Working Group I to the Sixth Assessment Report of the Intergovernmental Panel on Climate Change [Masson-Delmotte, V., P. Zhai, A. Pirani, S. L. Connors, C. Péan, S. Berger, N. Caud, Y. Chen, L. Goldfarb, M. I. Gomis, M. Huang, K. Leitzell, E. Lonnoy, J.B.R. Matthews, T. K. Maycock, T. Waterfield, O. Yelekçi, R. Yu and B. Zhou (eds.)]. Cambridge University Press, 2021.

Jacobson, M. Z.: Control of fossil-fuel particulate black carbon and organic matter, possibly the most effective method of slowing global warming, J. Geophys. Res. Atmos., 107, https://doi.org10.1029/2001jd001376, 2002.

Jacobson, M. Z.: Short-term effects of controlling fossil-fuel soot, biofuel soot and gases, and methane on climate, Arctic ice, and air pollution health, J. Geophys. Res. Atmos., 115, https://doi.org10.1029/2009jd013795, 2010.

Ji, Z., Kang, S., Cong, Z., Zhang, Q., and Yao, T.: Simulation of carbonaceous aerosols over the Third Pole and adjacent regions: distribution, transportation, deposition, and climatic effects, Clim. Dyn., 45, 2831-2846, https://doi.org10.1007/s00382-015-2509-1, 2015.

Jiang, H. L. and Cotton, W. R.: A diagnostic study of subgrid-scale activation - art. no. D16107, J. Geophys. Res. Atmos., 110, https://doi.org10.1029/2004jd005722, 2005.

Johnson, K. S., Zuberi, B., Molina, L. T., Molina, M. J., Iedema, M. J., Cowin, J. P., Gaspar, D. J., Wang, C., and Laskin, A.: Processing of soot in an urban environment: case study from the Mexico City Metropolitan Area, Atmos. Chem. Phys., 5, 3033-3043, https://doi.org10.5194/acp-5-3033-2005, 2005.

Kanakidou, M., Seinfeld, J. H., Pandis, S. N., Barnes, I., Dentener, F. J., Facchini, M. C., Van Dingenen, R., Ervens, B., Nenes, A., Nielsen, C. J., Swietlicki, E., Putaud, J. P., Balkanski, Y., Fuzzi, S., Horth, J., Moortgat, G. K., Winterhalter, R., Myhre, C. E. L., Tsigaridis, K., Vignati, E., Stephanou, E. G., and Wilson, J.: Organic aerosol and global climate modelling: a review, Atmos. Chem. Phys., 5, 1053-1123, https://doi.org10.5194/acp-5-1053-2005, 2005.

Kasten, F.: Visibility in the prephase of condensation, Tellus, 21, 631-635, 1969.

Kiehl, J. T. and Briegleb, B. P.: The Relative Roles of Sulfate Aerosols and Greenhouse Gases in Climate Forcing, 260, 311-314, https://doi.orgdoi:10.1126/science.260.5106.311, 1993.

Kiehl, J. T., Schneider, T. L., Rasch, P. J., Barth, M. C., and Wong, J.: Radiative forcing due to sulfate aerosols from simulations with the National Center for Atmospheric Research Community Climate Model, Version 3, 105, 1441-1457, https://doi.org10.1029/1999JD900495, 2000.

Kiehl, J. T., Hack, J. J., Bonan, G. B., Boville, B. A., Briegleb, B. P., Williamson, D. L., and Rasch, P. J.: Description of the NCAR Community Climate Model (CCM3), University Corporation for Atmospheric Research, NCAR/TN-420+STR, https://doi.org10.5065/D6FF3Q99, 1996.

Koch, D. and Del Genio, A. D.: Black carbon semi-direct effects on cloud cover: review and synthesis, Atmos. Chem. Phys., 10, 7685-7696, https://doi.org10.5194/acp-10-7685-2010, 2010.

https://doi.org/10.5194/egusphere-2026-2776
Preprint. Discussion started: 15 June 2026

Koch, D., Bauer, S. E., Del Genio, A., Faluvegi, G., McConnell, J. R., Menon, S., Miller, R. L., Rind, D., Ruedy, R., Schmidt, G. A., and Shindell, D.: Coupled Aerosol-Chemistry-Climate Twentieth-Century Transient Model Investigation: Trends in Short-Lived Species and Climate Responses, J. Clim., 24, 2693-2714, https://doi.org10.1175/2011jcli3582.1, 2011.

Koch, D., Schulz, M., Kinne, S., McNaughton, C., Spackman, J. R., Balkanski, Y., Bauer, S., Berntsen, T., Bond, T. C., Boucher, O., Chin, M., Clarke, A., De Luca, N., Dentener, F., Diehl, T., Dubovik, O., Easter, R., Fahey, D. W., Feichter, J., Fillmore, D., Freitag, S., Ghan, S., Ginoux, P., Gong, S., Horowitz, L., Iversen, T., Kirkevag, A., Klimont, Z., Kondo, Y., Krol, M., Liu, X., Miller, R., Montanaro, V., Moteki, N., Myhre, G., Penner, J. E., Perlwitz, J., Pitari, G., Reddy, S., Sahu, L., Sakamoto, H., Schuster, G., Schwarz, J. P., Seland, O., Stier, P., Takegawa, N., Takemura, T., Textor, C., van Aardenne, J. A., and Zhao, Y.: Evaluation of black carbon estimations in global aerosol models, Atmos. Chem. Phys., 9, 9001-9026, https://doi.org10.5194/acp-9-9001-2009, 2009.

Krasowsky, T. S., McMeeking, G. R., Wang, D., Sioutas, C., and Ban-Weiss, G. A.: Measurements of the impact of atmospheric aging on physical and optical properties of ambient black carbon particles in Los Angeles, Atmos. Environ., 142, 496-504, https://doi.org10.1016/j.atmosenv.2016.08.010, 2016.

Lack, D. A., Langridge, J. M., Bahreini, R., Cappa, C. D., Middlebrook, A. M., and Schwarz, J. P.: Brown carbon and internal mixing in biomass burning particles, Proc. Nat. Acad. Sci., 109, 14802-14807, https://doi.org10.1073/pnas.1206575109, 2012.

Lee, Y. H., Lamarque, J. F., Flanner, M. G., Jiao, C., Shindell, D. T., Berntsen, T., Bisiaux, M. M., Cao, J., Collins, W. J., Curran, M., Edwards, R., Faluvegi, G., Ghan, S., Horowitz, L. W., McConnell, J. R., Ming, J., Myhre, G., Nagashima, T., Naik, V., Rumbold, S. T., Skeie, R. B., Sudo, K., Takemura, T., Thevenon, F., Xu, B., and Yoon, J. H.: Evaluation of preindustrial to present-day black carbon and its albedo forcing from Atmospheric Chemistry and Climate Model Intercomparison Project (ACCMIP) (vol 13, pg 2607, 2013), Atmos. Chem. Phys., 13, 6553-6554, https://doi.org10.5194/acp-13-6553-2013, 2013.

Li, J., Carlson, B. E., Yung, Y. L., Lv, D., Hansen, J., Penner, J. E., Liao, H., Ramaswamy, V., Kahn, R. A., Zhang, P., Dubovik, O., Ding, A., Lacis, A. A., Zhang, L., and Dong, Y.: Scattering and absorbing aerosols in the climate system, Nat. Rev. Earth Environ., 3, 363-379, https://doi.org10.1038/s43017-022-00296-7, 2022.

Li, K., Liao, H., Mao, Y., and Ridley, D. A.: Source sector and region contributions to concentration and direct radiative forcing of black carbon in China, Atmos. Environ., 124, 351-366, https://doi.org10.1016/j.atmosenv.2015.06.014, 2016.

Li, M., Liu, H., Geng, G., Hong, C., Liu, F., Song, Y., Tong, D., Zheng, B., Cui, H., Man, H., Zhang, Q., and He, K.: Anthropogenic emission inventories in China: a review, Natl. Sci. Rev., 4, 834-866, https://doi.org10.1093/nsr/nwx150, 2017a.

Li, M., Zhang, Q., Kurokawa, J.-i., Woo, J.-H., He, K., Lu, Z., Ohara, T., Song, Y., Streets, D. G., Carmichael, G. R., Cheng, Y., Hong, C., Huo, H., Jiang, X., Kang, S., Liu, F., Su, H., and Zheng, B.: MIX: a mosaic Asian anthropogenic emission inventory under the international collaboration framework of the MICS-Asia and HTAP, Atmos. Chem. Phys., 17, 935-963, https://doi.org10.5194/acp-17-935-2017, 2017b.

Li, M., Zhang, Q., Kurokawa, J., Woo, J. H., He, K. B., Lu, Z. F., Ohara, T., Song, Y., Streets, D. G., Carmichael, G. R., Cheng, Y. F., Hong, C. P., Huo, H., Jiang, X. J., Kang, S. C., Liu, F., Su, H., and Zheng, B.: MIX: a mosaic Asian anthropogenic emission inventory under the international collaboration framework of the MICS-Asia and HTAP, Atmos. Chem. Phys., 17, 935-963,

https://doi.org/10.5194/egusphere-2026-2776
Preprint. Discussion started: 15 June 2026

https://doi.org10.5194/acp-17-935-2017, 2017c.

Liou, K. N. and Ou, S. C.: THE ROLE OF CLOUD MICROPHYSICAL PROCESSES IN CLIMATE - AN ASSESSMENT FROM A ONE-DIMENSIONAL PERSPECTIVE, J. Geophys. Res. Atmos., 94, 8599-8607, https://doi.org10.1029/JD094iD06p08599, 1989.

Liu, X., Ma, P. L., Wang, H., Tilmes, S., Singh, B., Easter, R. C., Ghan, S. J., and Rasch, P. J.: Description and evaluation of a new four-mode version of the Modal Aerosol Module (MAM4) within version 5.3 of the Community Atmosphere Model, Geosci. Model Dev., 9, 505-522, https://doi.org10.5194/gmd-9-505-2016, 2016.

Liu, Y., Wang, M., Qian, Y., and Ding, A.: A Strong Anthropogenic Black Carbon Forcing Constrained by Pollution Trends Over China, Geophys. Res. Lett., 49, https://doi.org10.1029/2022gl098965, 2022.

Liu, Y. G. and Daum, P. H.: Anthropogenica erosols - Indirect warming effect from dispersion forcing, Nature, 419, 580-581, https://doi.org10.1038/419580a, 2002.

Liu, Z., Cohen, J. B., Wang, S., Wang, X., Tiwari, P., and Qin, K.: Remotely sensed BC columns over rapidly changing Western China show significant decreases in mass and inconsistent changes in number, size, and mixing properties due to policy actions, npj Clim. Atmos. Sci., 7, https://doi.org10.1038/s41612-024-00663-9, 2024.

Liu, Z., Cohen, J. B., Tiwari, P., Guan, L., Wang, S., Li, Z., and Qin, K.: A global black carbon dataset of column concentration and microphysical information derived from MISR multi-band observations and Mie scattering simulations, Earth Syst. Sci. Data, 18, 507-533, https://doi.org10.5194/essd-18-507-2026, 2026.

Lohmann, U., Feichter, J., Chuang, C. C., and Penner, J. E.: Prediction of the number of cloud droplets in the ECHAM GCM, J. Geophys. Res.: Atmos., 104, 9169-9198, https://doi.orghttps://doi.org/10.1029/1999JD900046, 1999.

Lund, M. T., Berntsen, T. K., and Samset, B. H.: Sensitivity of black carbon concentrations and climate impact to aging and scavenging in OsloCTM2-M7, Atmos. Chem. Phys., 17, 6003-6022, https://doi.org10.5194/acp-17-6003-2017, 2017.

Lund, M. T., Samset, B. H., Skeie, R. B., Watson-Parris, D., Katich, J. M., Schwarz, J. P., and Weinzierl, B.: Short Black Carbon lifetime inferred from a global set of aircraft observations, npj Clim. Atmos. Sci., 1, https://doi.org10.1038/s41612-018-0040-x, 2018.

Ma, D. Y., Wang, T. J., Xu, B. Y., Song, R., Gao, L. B., Chen, H. M., Ren, X. J., Li, S., Zhuang, B. L., Li, M. M., Xie, M., and Saikawa, E.: The mutual interactions among ozone, fine particulate matter, and carbon dioxide on summer monsoon climate in East Asia, Atmos. Environ., 299, https://doi.org10.1016/j.atmosenv.2023.119668, 2023.

Martin, G. M., Johnson, D. W., and Spice, A.: THE MEASUREMENT AND PARAMETERIZATION OF EFFECTIVE RADIUS OF DROPLETS IN WARM STRATOCUMULUS CLOUDS, J. Atmos. Sci., 51, 1823-1842, https://doi.org10.1175/1520-0469(1994)051<1823:Tmapoe>2.0.Co;2, 1994.

Matzler, C.: MATLAB functions for Mie scattering and absorption, IAP Res Rep, 8, 2002.

McFiggans, G., Artaxo, P., Baltensperger, U., Coe, H., Facchini, M. C., Feingold, G., Fuzzi, S., Gysel, M., Laaksonen, A., Lohmann, U., Mentel, T. F., Murphy, D. M., O'Dowd, C. D., Snider, J. R., and Weingartner, E.: The effect of physical and chemical aerosol properties on warm cloud droplet activation, Atmos. Chem. Phys., 6, 2593-2649, https://doi.org10.5194/acp-6-2593-2006, 2006.

Menon, S., Hansen, J., Nazarenko, L., and Luo, Y. F.: Climate effects of black carbon aerosols in China and India, Science, 297, 2250-2253, https://doi.org10.1126/science.1075159, 2002.

https://doi.org/10.5194/egusphere-2026-2776
Preprint. Discussion started: 15 June 2026

Moffet, R. C. and Prather, K. A.: In-situ measurements of the mixing state and optical properties of soot with implications for radiative forcing estimates, Proc. Nat. Acad. Sci., 106, 11872-11877, https://doi.org10.1073/pnas.0900040106, 2009.

Myhre, G., Samset, B. H., Schulz, M., Balkanski, Y., Bauer, S., Berntsen, T. K., Bian, H., Bellouin, N., Chin, M., Diehl, T., Easter, R. C., Feichter, J., Ghan, S. J., Hauglustaine, D., Iversen, T., Kinne, S., Kirkevåg, A., Lamarque, J. F., Lin, G., Liu, X., Lund, M. T., Luo, G., Ma, X., van Noije, T., Penner, J. E., Rasch, P. J., Ruiz, A., Seland, O., Skeie, R. B., Stier, P., Takemura, T., Tsigaridis, K., Wang, P., Wang, Z., Xu, L., Yu, H., Yu, F., Yoon, J. H., Zhang, K., Zhang, H., and Zhou, C.: Radiative forcing of the direct aerosol effect from AeroCom Phase II simulations, Atmos. Chem. Phys., 13, 1853-1877, https://doi.org10.5194/acp-13-1853-2013, 2013.

Nair, V. S., Solmon, F., Giorgi, F., Mariotti, L., Babu, S. S., and Moorthy, K. K.: Simulation of South Asian aerosols for regional climate studies, J. Geophys. Res.: Atmos., 117, https://doi.org10.1029/2011jd016711, 2012.

Ocko, I. B., Ramaswamy, V., Ginoux, P., Ming, Y., and Horowitz, L. W.: Sensitivity of scattering and absorbing aerosol direct radiative forcing to physical climate factors, J. Geophys. Res.: Atmos., 117, https://doi.org10.1029/2012jd018019, 2012.

Ohata, S., Moteki, N., Mori, T., Koike, M., and Kondo, Y.: A key process controlling the wet removal of aerosols: new observational evidence, Sci. Rep., 6, https://doi.org10.1038/srep34113, 2016.

Park, R. J., Jacob, D. J., Chin, M., and Martin, R. V.: Sources of carbonaceous aerosols over the United States and implications for natural visibility - art. no. 4355, J. Geophys. Res.: Atmos., 108, https://doi.org10.1029/2002jd003190, 2003.

Peng, J., Hu, M., Guo, S., Du, Z., Zheng, J., Shang, D., Zamora, M., Zeng, L., Shao, M., Wu, Y., Zheng, J., Wang, Y., Glen, C., Collins, D., Molina, M., and Zhang, R.: Markedly enhanced absorption and direct radiative forcing of black carbon under polluted urban environments, Proc. Nat. Acad. Sci., 252, 2016.

Petters, M. D. and Kreidenweis, S. M.: A single parameter representation of hygroscopic growth and cloud condensation nucleus activity, Atmos. Chem. Phys., 7, 1961-1971, https://doi.org10.5194/acp-7-1961-2007, 2007.

Qian, Y., Giorgi, F., Huang, Y., Chameides, W., and Luo, C.: Regional simulation of anthropogenic sulfur over East Asia and its sensitivity to model parameters, Tellus Series B-Chemical and Physical Meteorology, 53, 171-191, https://doi.org10.1034/j.1600-0889.2001.d01-14.x, 2001.

Qie, K., Tian, W., Bian, J., Xie, F., and Li, D.: Weakened Asian summer monsoon anticyclone related to increased anthropogenic aerosol emissions in recent decades, npj Clim. Atmos. Sci., 8, https://doi.org10.1038/s41612-025-01026-8, 2025.

Ramanathan, V. and Carmichael, G.: Global and regional climate changes due to black carbon, Nat. Geosci., 1, 221-227, https://doi.org10.1038/ngeo156, 2008.

Randles, C. A. and Ramaswamy, V.: Absorbing aerosols over Asia: A Geophysical Fluid Dynamics Laboratory general circulation model sensitivity study of model response to aerosol optical depth and aerosol absorption, J. Geophys. Res.: Atmos., 113, https://doi.org10.1029/2008jd010140, 2008.

Reutter, P., Su, H., Trentmann, J., Simmel, M., Rose, D., Gunthe, S. S., Wernli, H., Andreae, M. O., and Poeschl, U.: Aerosol- and updraft-limited regimes of cloud droplet formation: influence of particle number, size and hygroscopicity on the activation of cloud condensation nuclei (CCN), Atmos. Chem. Phys., 9, 7067-7080, https://doi.org10.5194/acp-9-7067-2009, 2009.

Riemer, N., Vogel, H., and Vogel, B.: Soot aging time scales in polluted regions during day and night,

https://doi.org/10.5194/egusphere-2026-2776
Preprint. Discussion started: 15 June 2026

Atmos. Chem. Phys., 4, 1885-1893, https://doi.org10.5194/acp-4-1885-2004, 2004.

Riemer, N., West, M., Zaveri, R. A., and Easter, R. C.: Simulating the evolution of soot mixing state with a particle-resolved aerosol model, J. Geophys. Res.: Atmos., 114, https://doi.org10.1029/2008jd011073, 2009.

Riemer, N., Ault, A. P., West, M., Craig, R. L., and Curtis, J. H.: Aerosol Mixing State: Measurements, Modeling, and Impacts, Rev. Geophys., 57, 187-249, https://doi.org10.1029/2018rg000615, 2019.

Sand, M., Samset, B. H., Myhre, G., Gliss, J., Bauer, S. E., Bian, H. S., Chin, M. A., Checa-Garcia, R., Ginoux, P., Kipling, Z., Kirkevåg, A., Kokkola, H., Le Sager, P., Lund, M. T., Matsui, H., van Noije, T., Olivié, D. J. L., Remy, S., Schulz, M., Stier, P., Stjern, C. W., Takemura, T., Tsigaridis, K., Tsyro, S. G., and Watson-Parris, D.: Aerosol absorption in global models from AeroCom phase III, Atmos. Chem. Phys., 21, 15929-15947, https://doi.org10.5194/acp-21-15929-2021, 2021.

Shalaby, A., Zakey, A. S., Tawfik, A. B., Solmon, F., Giorgi, F., Stordal, F., Sillman, S., Zaveri, R. A., and Steiner, A. L.: Implementation and evaluation of online gas-phase chemistry within a regional climate model (RegCM-CHEM4), Geosci. Model Dev., 5, 741-760, https://doi.org10.5194/gmd-5-741-2012, 2012.

Shen, W., Wang, M., Riemer, N., Zheng, Z., Liu, Y., and Dong, X.: Improving BC Mixing State and CCN Activity Representation With Machine Learning in the Community Atmosphere Model Version 6 (CAM6), J. Adv. Model. Earth Syst., 16, https://doi.org10.1029/2023ms003889, 2024.

Shen, W., Wang, M., Liu, Y., Dong, X., Zhao, D., Yue, M., Tian, P., and Ding, D.: Evaluating BC Aging Processes in the Community Atmosphere Model Version 6 (CAM6), J. Geophys. Res.: Atmos., 128, https://doi.org10.1029/2022jd037427, 2023.

Shen, Z., Liu, J., Horowitz, L. W., Henze, D. K., Fan, S., Levy, H., II, Mauzerall, D. L., Lin, J. T., and Tao, S.: Analysis of transpacific transport of black carbon during HIPPO-3: implications for black carbon aging, Atmos. Chem. Phys., 14, 6315-6327, https://doi.org10.5194/acp-14-6315-2014, 2014.

Shindell, D. and Faluvegi, G.: Climate response to regional radiative forcing during the twentieth century, Nat. Geosci., 2, 294-300, https://doi.org10.1038/ngeo473, 2009.

Smith, C. J., Kramer, R. J., Myhre, G., Forster, P. M., Soden, B. J., Andrews, T., Boucher, O., Faluvegi, G., Flaschner, D., Hodnebrog, O., Kasoar, M., Kharin, V., Kirkevag, A., Lamarque, J. F., Muelmenstaedt, J., Olivie, D., Richardson, T., Samset, B. H., Shindell, D., Stier, P., Takemura, T., Voulgarakis, A., and Watson-Parris, D.: Understanding Rapid Adjustments to Diverse Forcing Agents, Geophys. Res. Lett., 45, 12023-12031, https://doi.org10.1029/2018gl079826, 2018.

Solmon, F., Giorgi, F., and Liousse, C.: Aerosol modelling for regional climate studies: application to anthropogenic particles and evaluation over a European/African domain, Tellus Series B-Chemical and Physical Meteorology, 58, 51-72, https://doi.org10.1111/j.1600-0889.2005.00155.x, 2006.

Stjern, C. W., Samset, B. H., Myhre, G., Forster, P. M., Hodnebrog, O., Andrews, T., Boucher, O., Faluvegi, G., Iversen, T., Kasoar, M., Kharin, V., Kirkevag, A., Lamarque, J.-F., Olivie, D., Richardson, T., Shawki, D., Shindell, D., Smith, C. J., Takemura, T., and Voulgarakis, A.: Rapid Adjustments Cause Weak Surface Temperature Response to Increased Black Carbon Concentrations, J. Geophys. Res.: Atmos., 122, 11462-11481, https://doi.org10.1002/2017jd027326, 2017.

Storelvmo, T.: Uncertainties in aerosol direct and indirect effects attributed to uncertainties in convective transport parameterizations, Atmos. Res., 118, 357-369, https://doi.org10.1016/j.atmosres.2012.06.022, 2012.

Sullivan, S. C., Lee, D., Oreopoulos, L., and Nenes, A.: Role of updraft velocity in temporal variability of global cloud hydrometeor number, Proc. Nat. Acad. Sci., 113, 5791-5796,

https://doi.org/10.5194/egusphere-2026-2776
Preprint. Discussion started: 15 June 2026

https://doi.org10.1073/pnas.1514039113, 2016.

Sun, H., Pan, Z., and Liu, X.: Numerical simulation of spatial-temporal distribution of dust aerosol and its direct radiative effects on East Asian climate, J. Geophys. Res.: Atmos., 117, https://doi.org10.1029/2011jd017219, 2012.

Takemura, T., Nozawa, T., Emori, S., Nakajima, T. Y., and Nakajima, T.: Simulation of climate response to aerosol direct and indirect effects with aerosol transport-radiation model - art. no. D02202, J. Geophys. Res.: Atmos., 110, https://doi.org10.1029/2004jd005029, 2005.

Tiwari, P., Cohen, J. B., Lu, L., Wang, S., Li, X., Guan, L., Liu, Z., Li, Z., and Qin, K.: Multi-platform observations and constraints reveal overlooked urban sources of black carbon in Xuzhou and Dhaka, Commun. Earth Environ., 6, https://doi.org10.1038/s43247-025-02012-x, 2025.

Twomey, S.: INFLUENCE OF POLLUTION ON SHORTWAVE ALBEDO OF CLOUDS, J. Atmos. Sci., 34, 1149-1152, https://doi.org10.1175/1520-0469(1977)034<1149:Tiopot>2.0.Co;2, 1977.

Virtanen, A., Joutsensaari, J., Kokkola, H., Partridge, D. G., Blichner, S., Seland, O., Holopainen, E., Tovazzi, E., Lipponen, A., Mikkonen, S., Leskinen, A., Hyvaerinen, A.-P., Zieger, P., Krejci, R., Ekman, A. M. L., Riipinen, I., Quaas, J., and Romakkaniemi, S.: High sensitivity of cloud formation to aerosol changes, Nat. Geosci., 18, 289-295, https://doi.org10.1038/s41561-025-01662-y, 2025.

Wang, D., Zhu, B., Wang, H., and Sun, L.: Simulation study on the indirect effect of sulfate on the summer climate over the eastern China monsoon region, Sci. Rep., 11, https://doi.org10.1038/s41598-021-87832-5, 2021.

Wang, H., Easter, R. C., Rasch, P. J., Wang, M., Liu, X., Ghan, S. J., Qian, Y., Yoon, J. H., Ma, P. L., and Vinoj, V.: Sensitivity of remote aerosol distributions to representation of cloud-aerosol interactions in a global climate model, Geosci. Model Dev., 6, 765-782, https://doi.org10.5194/gmd-6-765-2013, 2013.

Wang, J., Wang, J., Cai, R., Liu, C., Jiang, J., Nie, W., Wang, J., Moteki, N., Zaveri, R. A., Huang, X., Ma, N., Chen, G., Wang, Z., Jin, Y., Cai, J., Zhang, Y., Chi, X., Holanda, B. A., Xing, J., Liu, T., Qi, X., Wang, Q., Poehlker, C., Su, H., Cheng, Y., Wang, S., Hao, J., Andreae, M. O., and Ding, A.: Unified theoretical framework for black carbon mixing state allows greater accuracy of climate effect estimation, Nat. Commun., 14, https://doi.org10.1038/s41467-023-38330-x, 2023.

Wang, M. and Penner, J. E.: Aerosol indirect forcing in a global model with particle nucleation, Atmos. Chem. Phys., 9, 239-260, https://doi.org10.5194/acp-9-239-2009, 2009.

Wang, T. J., Zhuang, B. L., Li, S., Liu, J., Xie, M., Yin, C. Q., Zhang, Y., Yuan, C., Zhu, J. L., Ji, L. Q., and Han, Y.: The interactions between anthropogenic aerosols and the East Asian summer monsoon using RegCCMS, J. Geophys. Res.: Atmos., 120, 5602-5621, https://doi.org10.1002/2014jd022877, 2015.

Wang, Z., Lei, Y., Che, H., Wu, B., and Zhang, X.: Aerosol forcing regulating recent decadal change of summer water vapor budget over the Tibetan Plateau, Nat. Commun., 15, https://doi.org10.1038/s41467-024-46635-8, 2024.

Watson-Parris, D. and Smith, C. J.: Large uncertainty in future warming due to aerosol forcing, Nat. Clim. Change, 12, 1111-1113, https://doi.org10.1038/s41558-022-01516-0, 2022.

Weingartner, E., Burtscher, H., and Baltensperger, U.: Hygroscopic properties of carbon and diesel soot particles, Atmos. Environ., 31, 2311-2327, https://doi.org10.1016/s1352-2310(97)00023-x, 1997.

Wu, Y., Liu, D., Wang, J., Shen, F., Chen, Y., Cui, S., Ge, S., Wu, Y., Chen, M., and Ge, X.: Characterization of Size-Resolved Hygroscopicity of Black Carbon-Containing Particle in Urban Environment, Environ. Sci. Technol., 53, 14212-14221, https://doi.org10.1021/acs.est.9b05546,

https://doi.org/10.5194/egusphere-2026-2776
Preprint. Discussion started: 15 June 2026

2019.

Yang, Y., Ni, C., Jiang, M., and Chen, Q.: Effects of aerosols on the atmospheric boundary layer temperature inversion over the Sichuan Basin, China, Atmos. Environ., 262, https://doi.org10.1016/j.atmosenv.2021.118647, 2021.

Yang, Y., Wang, H., Smith, S. J., Ma, P.-L., and Rasch, P. J.: Source attribution of black carbon and its direct radiative forcing in China, Atmos. Chem. Phys., 17, 4319-4336, https://doi.org10.5194/acp-17-4319-2017, 2017.

Yin, C., Wang, T., Solmon, F., Mallet, M., Jiang, F., Li, S., and Zhuang, B.: Assessment of direct radiative forcing due to secondary organic aerosol over China with a regional climate model, Tellus Series B-Chemical and Physical Meteorology, 67, https://doi.org10.3402/tellusb.v67.24634, 2015.

Zakey, A. S., Giorgi, F., and Bi, X.: Modeling of sea salt in a regional climate model: Fluxes and radiative forcing, J. Geophys. Res.: Atmos., 113, https://doi.org10.1029/2007jd009209, 2008.

Zhang, H., Wang, Z., Guo, P., and Wang, Z.: A Modeling Study of the Effects of Direct Radiative Forcing Due to Carbonaceous Aerosol on the Climate in East Asia, Adv. Atmos. Sci., 26, 57-66, https://doi.org10.1007/s00376-009-0057-5, 2009.

Zhang, J., Liu, J., Tao, S., and Ban-Weiss, G. A.: Long-range transport of black carbon to the Pacific Ocean and its dependence on aging timescale, Atmos. Chem. Phys., 15, 11521-11535, https://doi.org10.5194/acp-15-11521-2015, 2015.

Zhang, Z., Wang, J., Riemer, N., Wang, J., Liu, C., Jin, Y., Tian, Z., Shen, S., Wang, B., Chen, G., Zhao, B., Hu, J., Wang, M., Su, H., Wang, S., Cheng, Y., and Ding, A.: The Droplet Activation Parameterization for Black Carbon-Containing Particles in Steady State, Geophys. Res. Lett., 52, https://doi.org10.1029/2024gl114433, 2025.

Zhao, S. and Suzuki, K.: Differing Impacts of Black Carbon and Sulfate Aerosols on Global Precipitation and the ITCZ Location via Atmosphere and Ocean Energy Perturbations, J. Clim., 32, 5567-5582, https://doi.org10.1175/jcli-d-18-0616.1, 2019.

Zheng, B., Tong, D., Li, M., Liu, F., Hong, C., Geng, G., Li, H., Li, X., Peng, L., Qi, J., Yan, L., Zhang, Y., Zhao, H., Zheng, Y., He, K., and Zhang, Q.: Trends in China's anthropogenic emissions since 2010 as the consequence of clean air actions, Atmos. Chem. Phys., 18, 14095-14111, https://doi.org10.5194/acp-18-14095-2018, 2018.

Zhou, Y., Huang, A., Jiang, J., and La, M.: Modeled interaction between the subseasonal evolving of the East Asian summer monsoon and the direct effect of anthropogenic sulfate, J. Geophys. Res.: Atmos., 119, 1993-2016, https://doi.org10.1002/2013jd020612, 2014.

Zhou, Y., Zhuang, B., Wang, T., Gao, P., Li, S., Hu, Y., Li, M., Cao, H., Xie, M., and Chen, H.: Characteristics of urban black carbon aerosols in the Yangtze River Delta of China based on long-term observations, Atmos. Environ., 326, https://doi.org10.1016/j.atmosenv.2024.120488, 2024.

Zhuang, B., Gao, Y., Hu, Y., Chen, H., Wang, T., Li, S., Li, M., and Xie, M.: Interaction between different mixing aerosol direct effects and East Asian summer monsoon, Clim. Dyn., 61, 1157-1176, https://doi.org10.1007/s00382-022-06617-2, 2023.

Zhuang, B., Liu, Q., Wang, T., Yin, C., Li, S., Xie, M., Jiang, F., and Mao, H.: Investigation on semi-direct and indirect climate effects of fossil fuel black carbon aerosol over China, Theor. Appl. Climatol., 114, 651-672, https://doi.org10.1007/s00704-013-0862-8, 2013.

Zhuang, B., Wang, T., Liu, J., Che, H., Han, Y., Fu, Y., Li, S., Xie, M., Li, M., Chen, P., Chen, H., Yang, X.-q., and Sun, J.: The optical properties, physical properties and direct radiative forcing of urban columnar aerosols in the Yangtze River Delta, China, Atmos. Chem. Phys., 18, 1419-1436,

https://doi.org/10.5194/egusphere-2026-2776
Preprint. Discussion started: 15 June 2026

https://doi.org10.5194/acp-18-1419-2018, 2018a.

Zhuang, B. L., Li, S., Wang, T. J., Liu, J., Chen, H. M., Chen, P. L., Li, M. M., and Xie, M.: Interaction between the Black Carbon Aerosol Warming Effect and East Asian Monsoon Using RegCM4, J. Clim., 31, 9367-9388, https://doi.org10.1175/jcli-d-17-0767.1, 2018b.

Zhuang, B. L., Chen, H. M., Li, S., Wang, T. J., Liu, J., Zhang, L. J., Liu, H. N., Xie, M., Chen, P. L., Li, M. M., and Zhao, M.: The direct effects of black carbon aerosols from different source sectors in East Asia in summer, Clim. Dyn., 53, 5293-5310, https://doi.org10.1007/s00382-019-04863-5, 2019.

Zhuang, B. L., Zhou, Y. A., Hu, Y. X., Liang, S. R., Gao, P., Gao, Y. M., Chen, H. M., Li, S., Wang, T. J., Xie, M., and Li, M. M.: Influence of ship emitted sulfur and carbonaceous aerosols on East Asian climate in summer, Atmos. Environ., 344, https://doi.org10.1016/j.atmosenv.2025.121035, 2025.

Zhuang, B. L., Wang, T. J., Li, S., Liu, J., Talbot, R., Mao, H. T., Yang, X. Q., Fu, C. B., Yin, C. Q., Zhu, J. L., Che, H. Z., and Zhang, X. Y.: Optical properties and radiative forcing of urban aerosols in Nanjing, China, Atmos. Environ., 83, 43-52, https://doi.org10.1016/j.atmosenv.2013.10.052, 2014.

Zou, Q., Zhu, L., Lu, C., Zhang, G. J., Xu, X., Chen, Q., and Li, D.: Parameterizations of different hydrometeor spectral relative dispersion in the convective clouds, Atmos. Oceanic Sci. Lett., 15, https://doi.org10.1016/j.aosl.2021.100141, 2022.

Zuberi, B., Johnson, K. S., Aleks, G. K., Molina, L. T., and Laskin, A.: Hydrophilic properties of aged soot - art. no. L01807, Geophys. Res. Lett., 32, https://doi.org10.1029/2004gl021496, 2005.